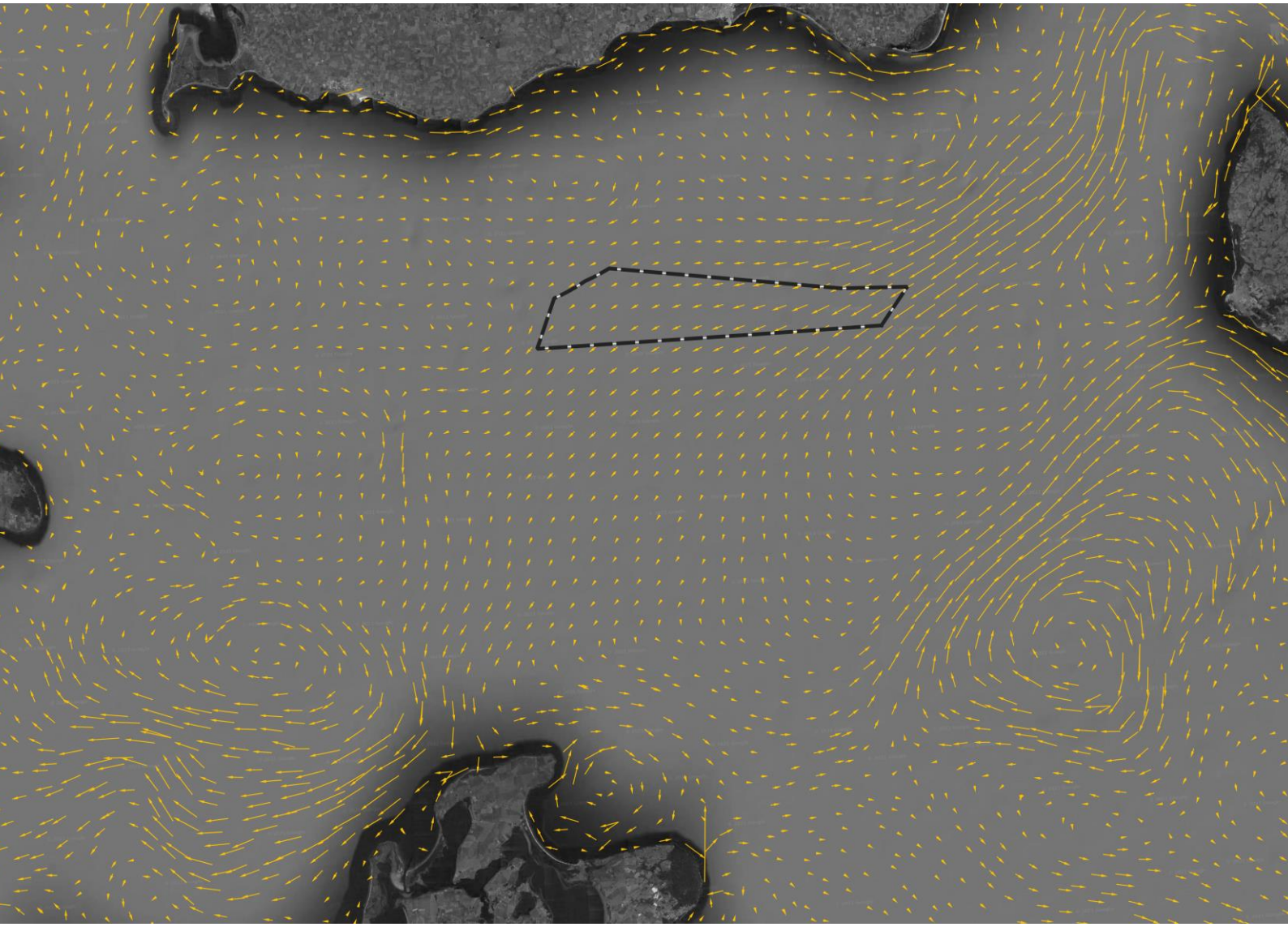

Triton OWF

Hydrodynamic Impact

OX2 AB

Date: 24 November 2021

Contents

Appendix

Rev. no.	Date	Description	Done by	Verified by	Approved by
3.28	10412485	Updated figures inclusive minor changes to the layout	TEB	KLBU	TEB

1 Introduction

OX2 plans to build an offshore wind farm 28 km south of Ystad, 35 km west of Ronne, 45 km north of Rygen and 58 km east of Mon in a rather flat area with a water depth of 45 m.

The planned wind farm is located in the Swedish part of the Baltic Sea 28 km south of Skåne and 35 km west of the Danish island Bornholm. The seabed in the wind farm area is rather flat and is around 45 m with some minor variations. It is planned to install up to 129 wind turbines on either monopiles, jackets or gravity-based substructures. Moreover to support the transmission of electricity or other types of energy up to 24 platforms may also be installed.

The purpose of the present study is to document the impact on the hydrodynamics, sediment transport and stratification due to the planned offshore wind farms Triton managed by OX2.

1.1 Abbreviations

ECMWF	European Center for Medium-range Weather Forecast
GBS	Gravity Based Substructure
OSS	Offshore substation
OWF	Offshore Wind Farm
PSU	Practical Salinity Unit
TP	Transition Piece

2 Summary

Project description

OX2 plans to build an offshore wind farm 28 km south of Ystad, 35 km west of Ronne, 45 km north of Rygen and 58 km east of Mon in a rather flat area with a water depth of 45 m. To investigate the impact on the hydrodynamics a worst-case scenario is used as a reference; a project with the layout for a 15 MW wind farm consisting of 129 turbines but with a conical gravity-based substructure for a 25 MW wind turbine, Figure 2.1. Moreover, for support of exporting the produced energy, potentially 24 platforms may be installed.

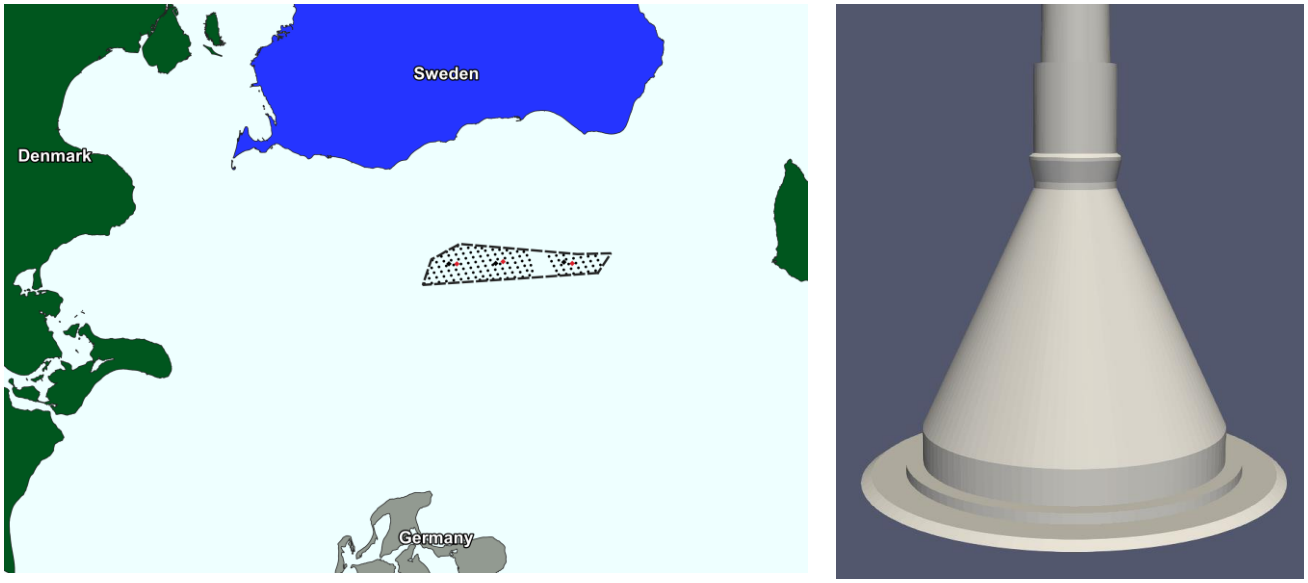

Figure 2.1: Project overview. Left: location of the Triton Offshore Wind Farm, Right: Conical gravity-based substructure with an ice cone.

For the general hydrodynamics, the largest impact is assumed to be caused by the gravity-based substructure due to the size of the cross-section area.

In terms of hydrodynamics and wave heights, the Triton Offshore Wind Farm mostly affects the flow pattern, current speeds and bed shear stresses.

Current

The flow pattern, which under average conditions travels from north-east to south-west, seems to be slightly switched towards west and south. This is described through the change in current speeds along with considering a mass balance of water entering and exiting the wind farm area. The former shows that wind turbines on the eastern part of the wind farm blocks the flow and leaves trails with reduced current speeds, whereas current speeds north of the OWF are found to increase slightly. The average current speeds are changed with up to 0.5 cm/s and the maximum current speeds with up to 2 cm/s. The latter confirms that there is a blockage associated with the presence of the wind farm even though this is very small.

Bed Shear Stresses

As the bed shear stresses are directly linked to the current speed, the change in bed shear stresses follows the change in the current speeds. I.e. the bed shear stresses are reduced in the eastern part of the offshore wind farm in case of annual averages and increased in between wind turbines when considering the maximum changes. It is assumed that the critical bed shear stress at the location of the Triton Offshore Wind Farm is in the range of 0.03 to 3 N/m^2. The presence of the wind farm causes changes to the annual average shear stresses and annual maximum shear stresses of around 0.001 and 0.01 N/m^2 respectively. As the background bed shear stress (the present shear stress) is 0.01 and 0.25 N/m^2 for the annual average and maximum, thus unlikely that the presence of the wind farm will lead to changes in the sediment transport neither in the wind farm area nor at the closest shore at Skåne (southern part of Sweden).

Waves

The wave heights, both annual averages and annual maximum wave heights are hardly affected at all due to the presence of the Triton OWF. It is estimated that the maximum impact on the significant wave height is limited to approximately 1 cm, which in terms of percentages is negligible when the average annual wave heights are 0.8 m and maximum annual wave heights are 3.75 mH_{m0} (both for the year 2016).

Flux

For the year 2016, the water balance for a box surrounding the wind farm in a distance of 6 to 15 km shows a reduction in the flux of 0.30%. This indicates that some water is being diverted due to the presence of the wind farm but that the blockage is negligible.

Stratification

For most of the time, the water column at the wind farm site is stratified with a low-density top layer (around 1005 kg/m^3) overlaying a bottom layer of 5 to 10 kg/m^3 heavier. Placement of a vertical structure across the water column will increase the amount of turbulence and potentially the amount of water being transported across the stratification e.g. increasing the salinity in the top and opposite in the bottom layer. At present the type of preferred substructure for the wind turbine hasn't been decided but three different types are considered: a gravity-based, a jacket and a monopile (Figure 2.2) whereof the latter is found to have the largest transport of water from the bottom to the top layer.

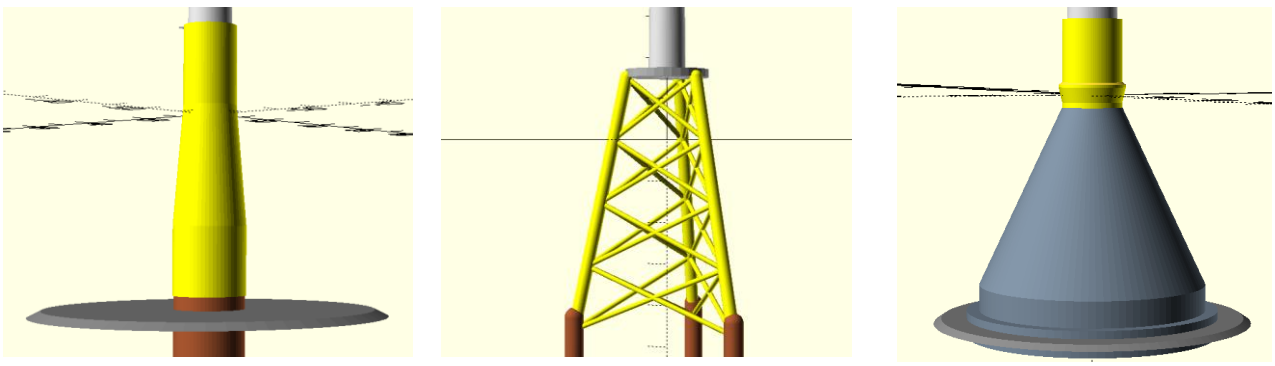

Figure 2.2: Sketch of the monopile, jacket and GBS used in the CFD model.

Based on statistical analyses of observed salinity, temperature, current speed and current direction on an hourly basis for the year 2014 to 2017 a conservative average impact to the salinity downstream (450 m) of the wind farm has been

estimated to be 0.3 PSU. This 0.3 PSU is approximately in the same order as the daily variations in the salinity observed at the Arkona Buoy in the top layers and a factor 2 to 3 times less of the daily changes in the lower layers.

The applied methodology is conservative in the sense that the changes in density occur just above the stratification and thus do not have an impact on the upper part of the top layer. The effect is in principle a small upwards local vertical movement of the stratification (pycnocline) downstream the substructure.

3 Methodology

A wind farm with its substructures and wind turbines may affect the current and wave pattern locally due to blocking from the substructure and further away as a combination of the blocking and a reduction in the wind from the wind turbine.

The Baltic Sea between Øresund/Femern and Bornholm where the Triton Offshore Wind Farm is located dominated by a stratified flow in the majority of the year with a pycnocline in around 36 below the sea surface which potentially may be affected by the increased turbulence generated by the substructures leading to changes in the salinity distribution.

To evaluate the impact of the wind farm on the hydrodynamics two types of numerical models are used. These are:

1) A far-field model for the description of the local and regional impact (from 50 m to more than 100 km) – see chapter 3.1 and
2) A near field model covering the foundation to a distance of 500 m, see chapter 3.2.

3.1 Impact, General hydrodynamics

Based on the general current pattern an average year in the period 2010 to 2020 is identified and used to determine the impact on the overall hydrodynamics due to the presence of the project.

The impact on the general hydrodynamics is done in 2 steps:

1) Executing of the regional model (the North Sea, Kattegat & Baltic Sea) for the baseline and with the project to get boundary data for the local model and the impact on the general flow.
2) Executing of the local model (Arkona Basin from Femern/Øresund to the west of Bornholm) again for both the baseline and the project to get the impact on
    a. The current
    b. The waves
    c. The local water balance
    d. The bed shear stresses

For the case with the project, the wind has been altered to reflect the losses of energy given by the wind turbines.

To simulate the current and waves the MIKE 21 hydrodynamic and wave spectral models are used. First for a case without the wind farm (baseline) and then for a case with the wind farm included. The relative impact is then found as the difference between the baseline case and the project case.

3.2 Impact, Stratification

Changes in the stratification due to increased mixing (turbulence) caused by the presence of the foundation is found by simulation of several selected cases with various boundary conditions e.g. levels of the pycnocline and densities/current speeds in the top and bottom layer. This is done with the use of the CFD model OpenFOAM.

1) Statistically analyses of data from the Marnet Arkona Basin; current and salinity at various water depths, for identification of variations in current vs. salinity and the level of the pycnocline;
2) Identification of the type of substructure with the largest impact on the mixing;
3) Simulation of selected events for an estimate of the yearly impact on the mixing with the worst-case substructure.
4) Accumulation of the impact by use of the statistical analyses and the impact from the events.

With the CFD model is it possible to simulate the turbulence downstream the substructure and thereby the size of the potential increased mixing and by comparison to a baseline e.g. a case with a substructure the relative impact.

4 Data

4.1 Project area

The Triton OWF is located at around 45 m of water 28 km south of Ystad, 35 km west of Ronne, 45 km north of Rygen and 58 km east of Mon, Figure 4.1.

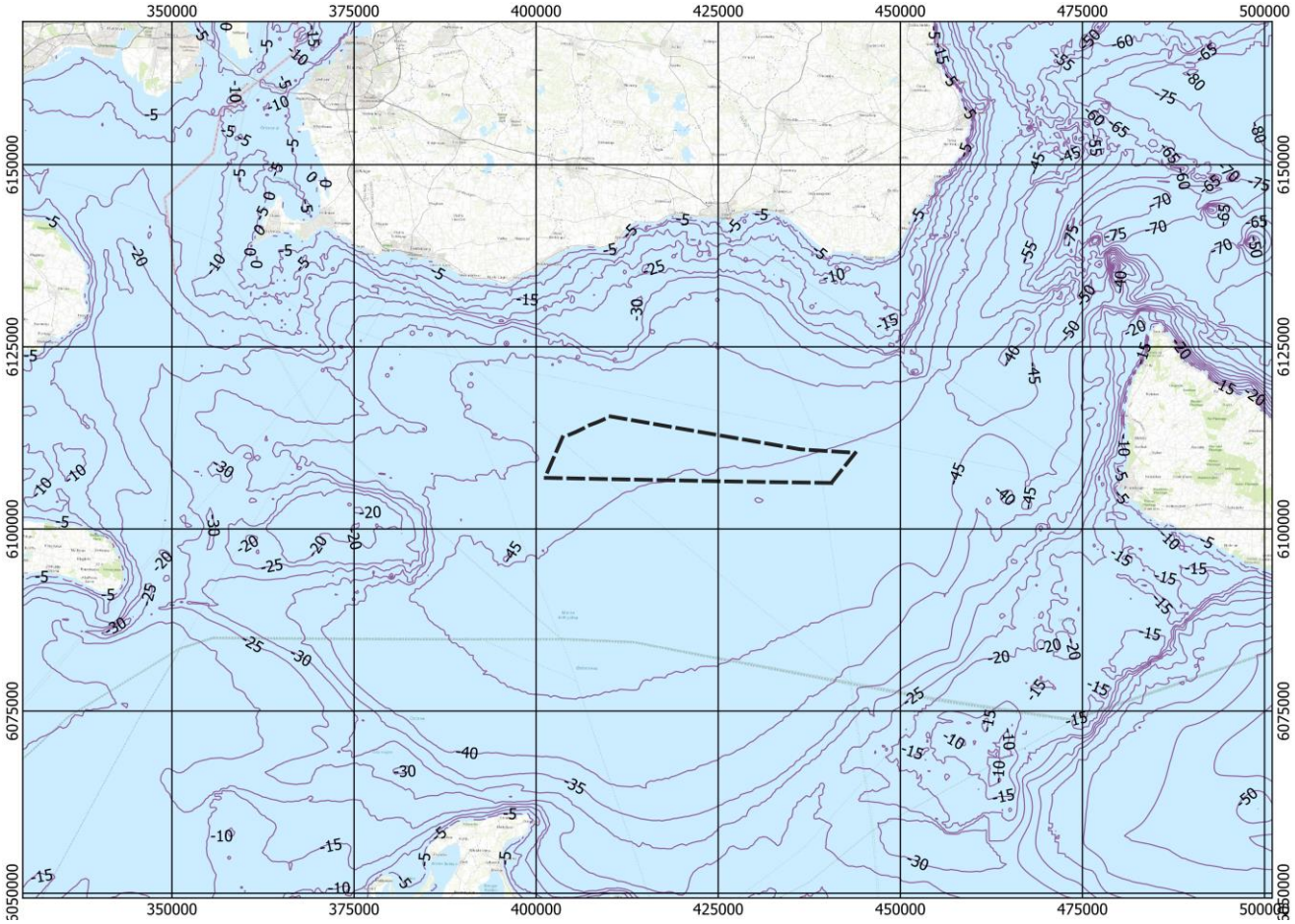

Figure 4.1: Triton OWF, location marked with 5 m contour curves (Baltic Sea Hydrographic Commission, 2020).

4.2 Wind farm layout

The wind farm layout is presented in Figure 4.2 and is referred to as the worst-case scenario in (NIRAS A/S, 2021), depicting A layout with 129 wind turbines on a foundation with the dimensions for a 25 MW foundations and 24 service platforms.

The layout showing 15MW locations of 25 MW substructures, OSS, platform, infield cables, ring cables and export cables are presented inFigure 4.2.

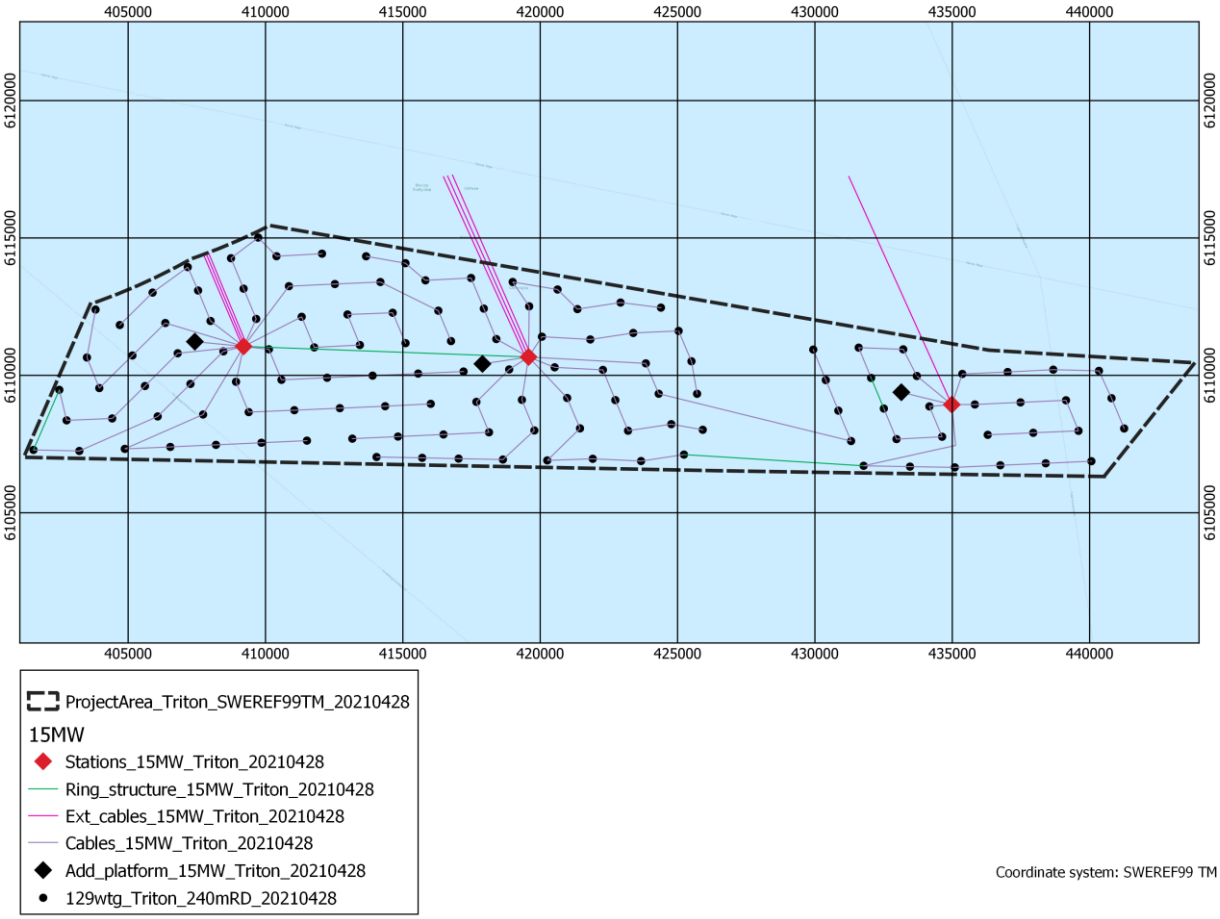

Figure 4.2: 15MW layout incl. infield cables, ring cables and a part of the export cables

The distance between the wind turbines is a minimum of 1200 m and up to 1680 m. The latter for the prevailing wind direction and the former perpendicular to the prevailing wind, Figure 4.3.

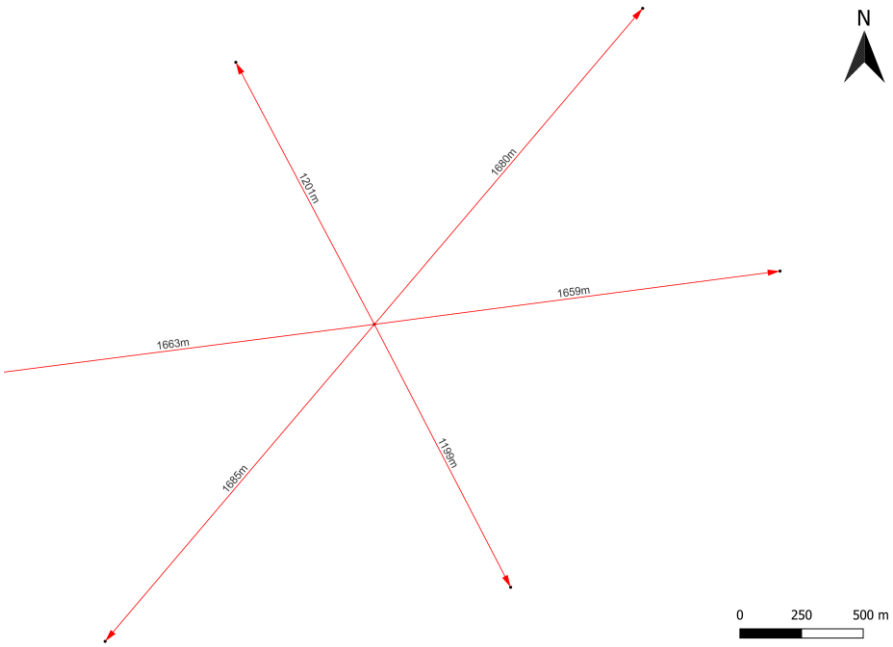

Figure 4.3: Typical distance between the wind turbines for the 15Mw layout

4.3 Substructure dimensions

The substructure type for the wind turbines is:

- a conical shaped Gravity Based Structure (GBS) with a base diameter of 45 m, a diameter of 12 m 2 m below sea level, an ice cone at sea level and hereafter a diameter of 12 m to the interface level 15 m above sea level. Around the base slab is placed a scour protection 1.5 m high to an extent of 10 m.
- a Jacket consisting of 3 legs with a diameter of 3 m, several braces with a diameter of 1.2 m and pin piles with a diameter of 4.5 m. The footprint at the seabed level is 45 m.
- a Monopile (MP) with a diameter at seabed level of 12 m, a transition piece (TP) from 3 m above the scour protection (1.5 m thick) to 15 m above sea level, TP diameter at interface level 10 m.

A sketch of the 3 types of substructure is shown in Figure 4.4 and Figure 4.5 on top of each other for comparison of the dimensions.

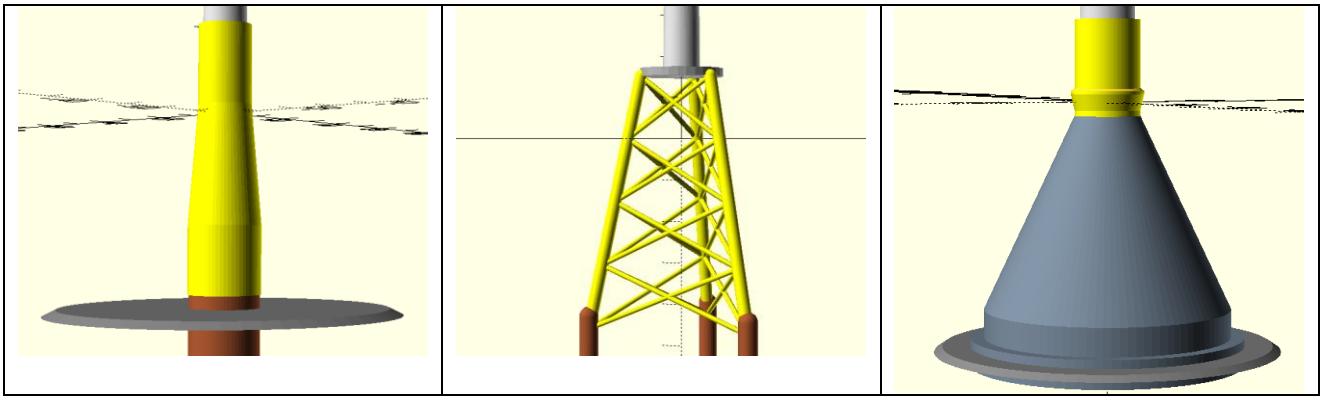

Figure 4.4: Sketch of the monopile, jacket and GBS used in the CFD model.

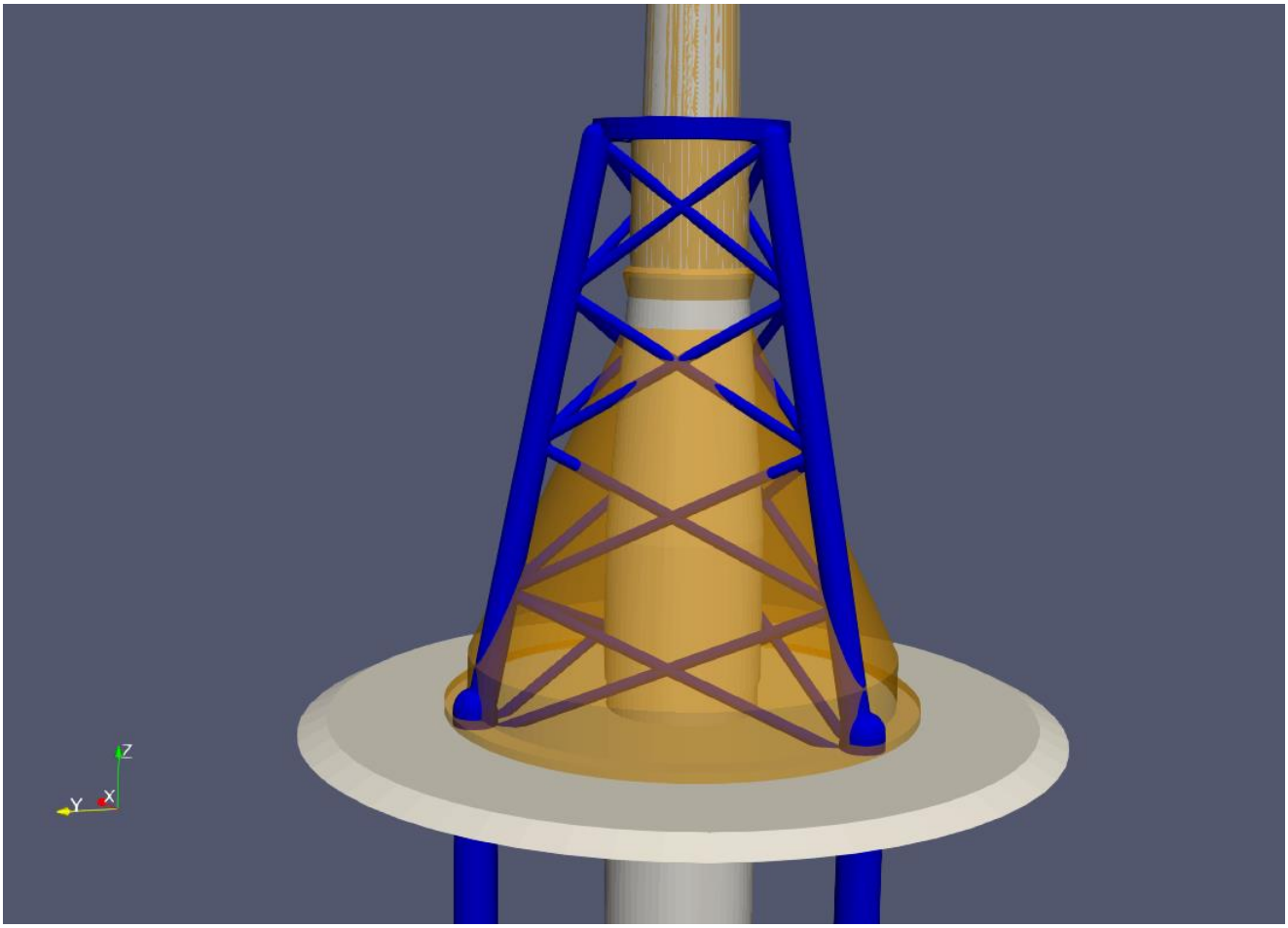

Figure 4.5: All 3 substructures on top of each other. MP: grey, GBS: orange and Jacket blue.

4.4 Bathymetry

Water depths in the model comes from various sources:

1) EMODnet bathymetry data (EMODnet, 2020);
2) Sea charts, Danish waters (Matrikelstyrelsen, 2012);
3) AIS data – inner Danish waters (Miljøministeriet, n.d.).
4) BSHC data – Baltic Sea (Baltic Sea Hydrographic Commission, 2020)

4.5 Wind

Atmospheric data in the form of wind speed in x and y-directions and air impact has been extracted from ECMWF (ECMWF, 2019). Data has a horizontal resolution of 0.5 degrees and 1 hour temporal.

4.6 Water level

At the model boundary towards the Atlantic Ocean, the tidal elevation is given as the astronomical tide along the boundary lines.

For verification of the hydrodynamic model, simulated and observed water levels are compared for Ystad, Gedser, Ronne, Kalmar and Visby (SMHI, Ladda ner oceanografiska observationer, 2019), cf. Section 5.3.

4.7 Discharge

Run-off from the most dominant catchment areas based on average values is included in the model. The data is downloaded from various homepages e.g. for Sweden Vattenweb (SMHI, vattenwebb, 2019). The sources considered in the model are illustrated in Figure 4.6.

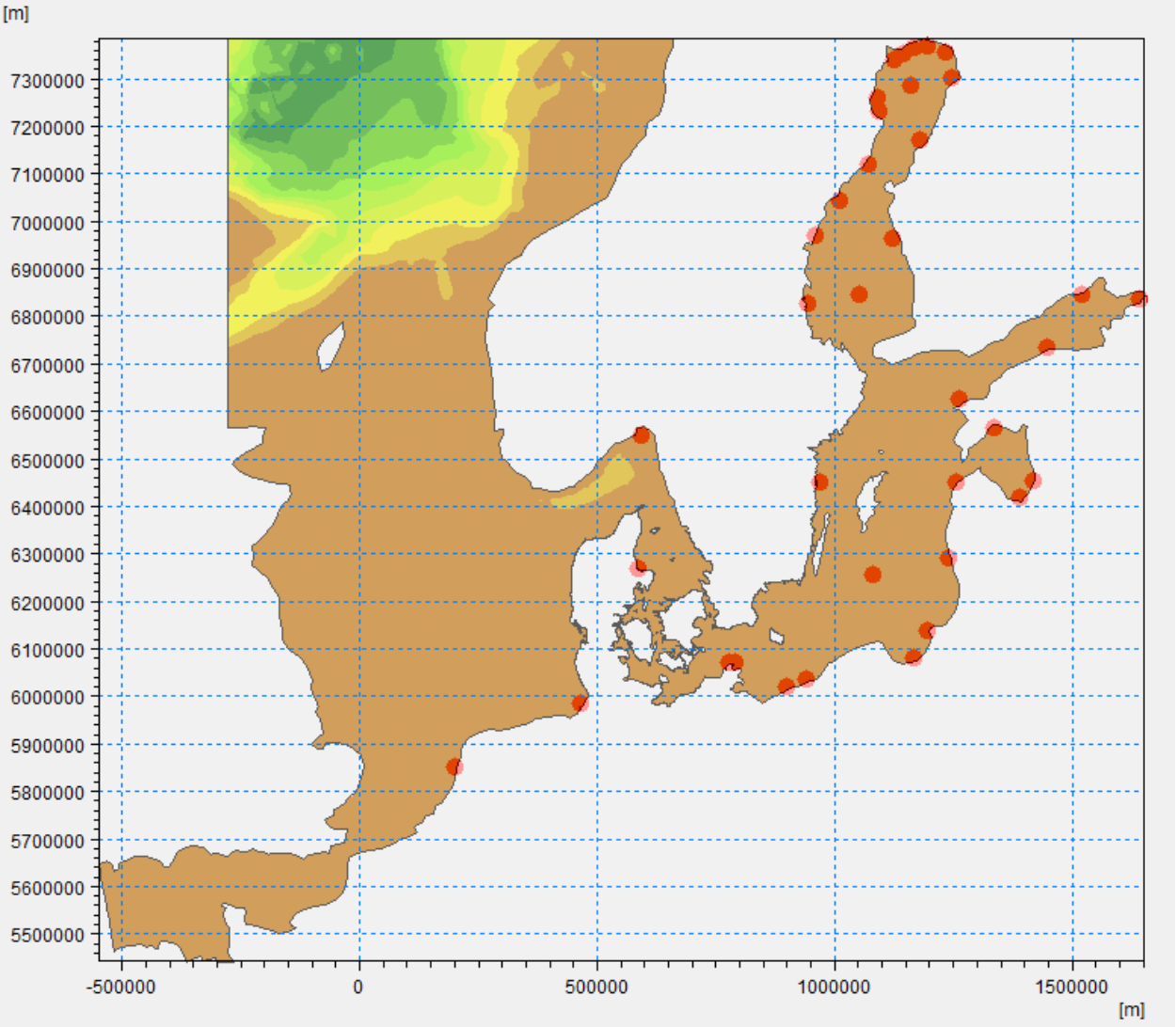

Figure 4.6: Most significant rivers (red dots) included in the MIKE21 models.

4.8 Current, salinity and temperature

Continuos data of current speed & direction, salinity and the water temperature has been measured by Leibniz-Institut für Ostseeforschung Warnemünde (IOW) on behalf of BSH (BSH, 2021) over the period 2014 to 2018 per 2 m between 4 m and 42 m for the current and the period 2014 to 2017 for salinity and temperature at 2, 5, 7, 16, 25, 33, 40 and 43 m. The floating platform is located at 54°53´N, 13°52´E at 45 m water approx. 25 km south of Triton OWF.

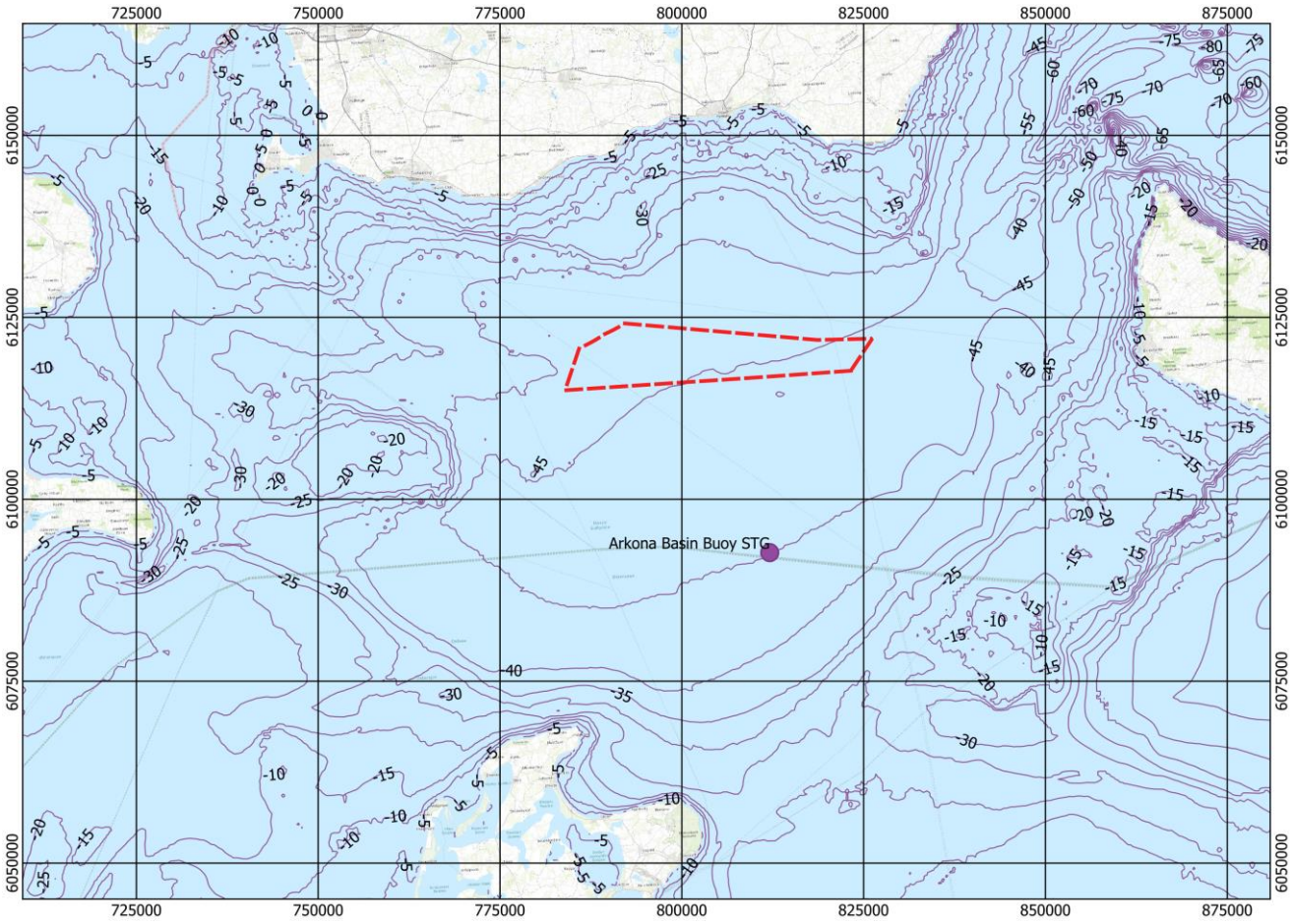

Figure 4.7: Location of the Marnet buoy Arkona Basin (purple dot) according to the Triton OWF (red dashed line).

The available data is presented in:

1) Appendix 4: Temperature profiles 2014 to 2017 incl. indication of termocline;
2) Appendix 5: Salinity profiles 2014 to 2017 incl. indication of halocline;
3) Appendix 6: Density profiles (calculated) 2014 to 2017 incl. indication of pycnocline;
4) Appendix 7: Current speed profiles 2014 to 2017 incl. indication of pycnocline;
5) Appendix 8: Current direction profiles 2014 to 2017 incl. indication of pycnocline.

For separation of potential layers in the water column, the pycnocline is assumed to best indication – strongest stratification.

The coverage with both temperature and salinity profiles is around 97% and for current speed/direction 82%.

5 General hydrodynamic model, setup and verification

5.1 Model extent and bathymetry

The calculation mesh is divided into several mesh sizes depending on the area of interest, Figure 5.1. The figure shows the extent of the model from the Baltic Sea in the east to the English Canal in the west and the North Sea towards the north.

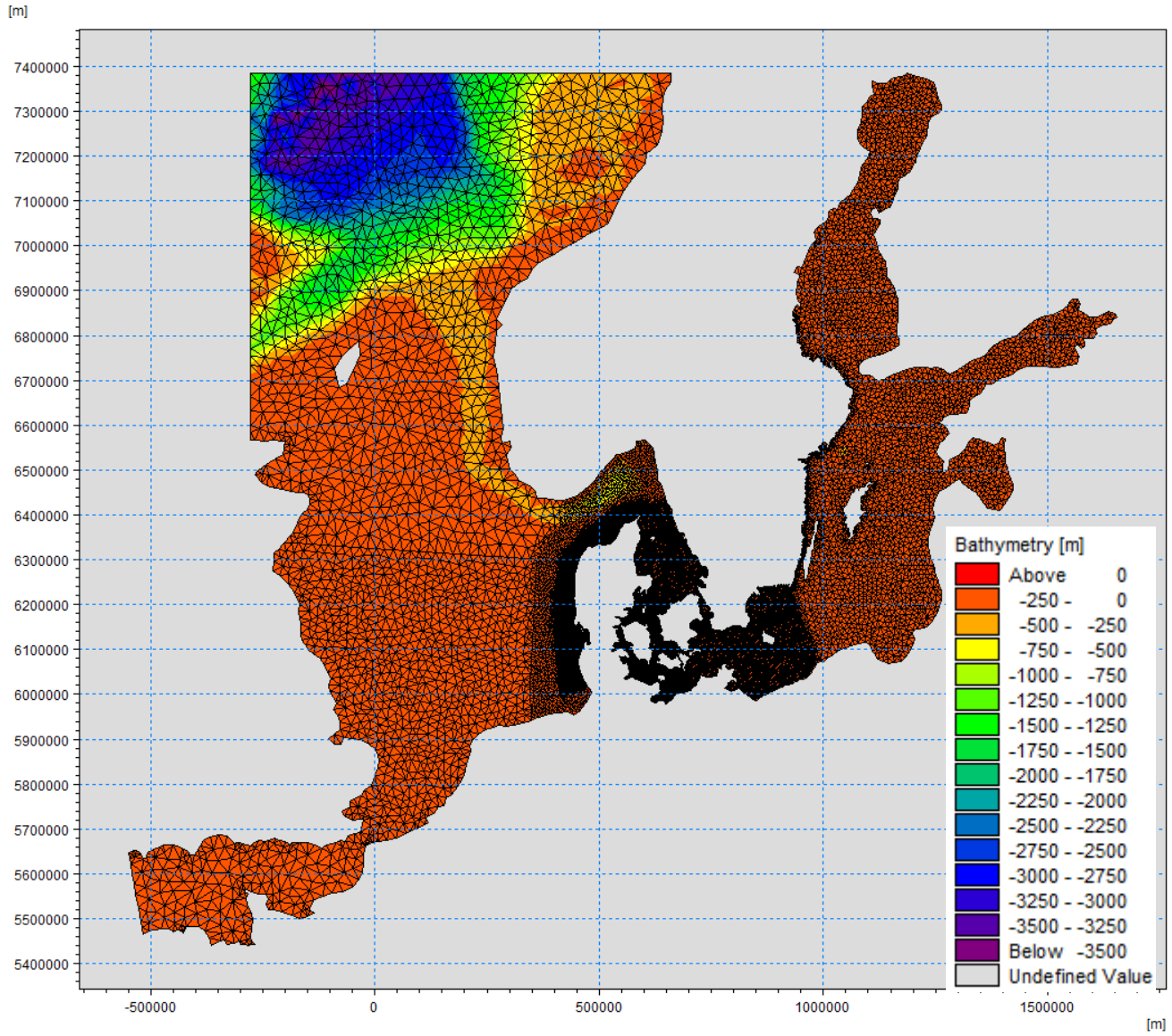

Figure 5.1: Mesh adoption for the MIKE21 Model

A closeup of the area around the Triton OWF is shown in Figure 5.2, where the finest mesh size extends from the wind farms to the Swedish coastline.

A sensitivity study has been made to investigate how far from the wind farm significant amounts of sediments are transported. The conclusion led to the mesh size and extend as shown in Figure 5.2.

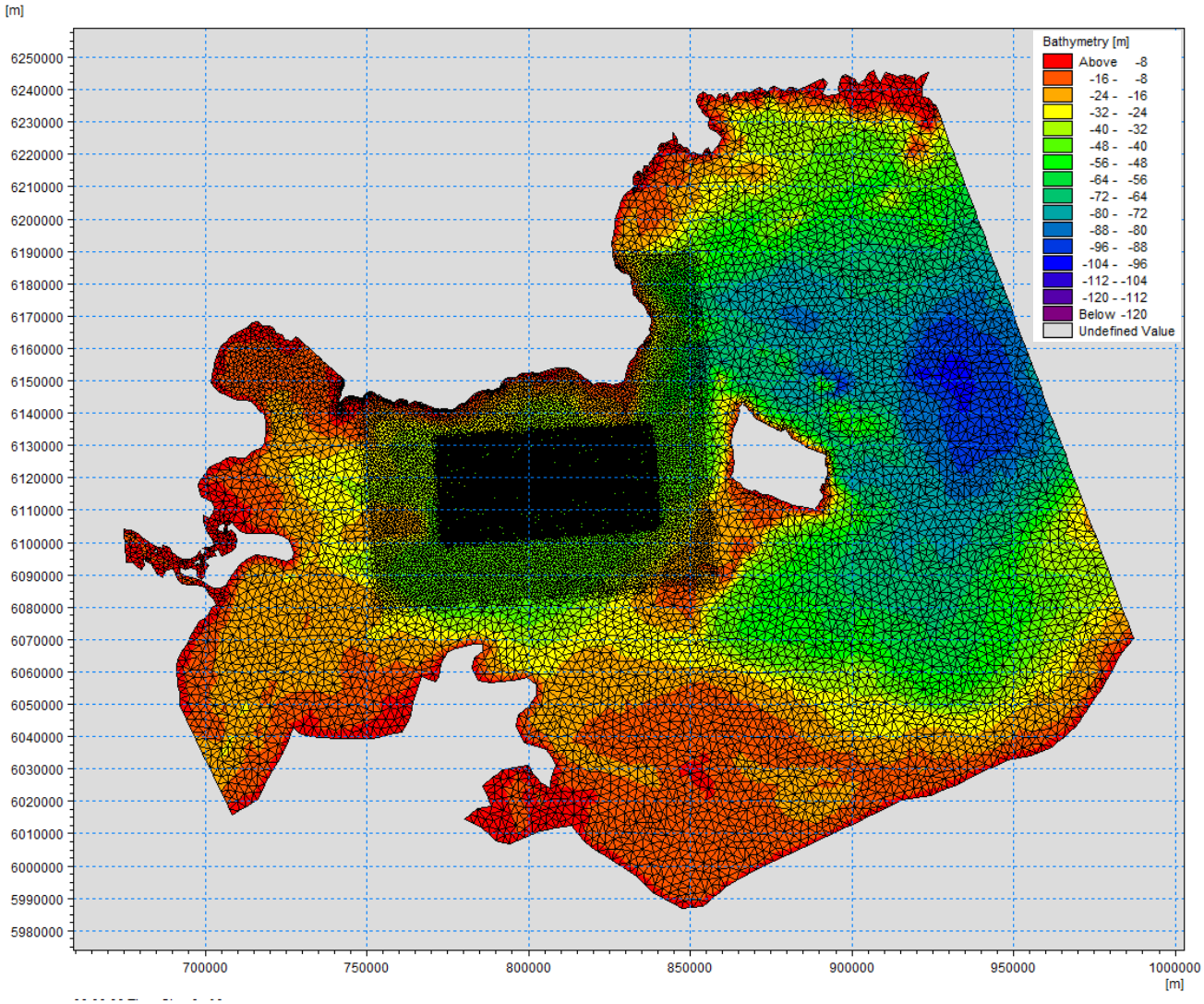

Figure 5.2: Local model mesh, wind farm site.

5.2 Boundary data

At the model boundary towards the Atlantic Ocean, the tidal elevation is given as the astronomical tide along the boundary lines.

For verification of the hydrodynamic model, simulated and observed water levels are compared for Ystad, Gedser, Ronne, Kalmar and Visby (SMHI, Ladda ner oceanografiska observationer, 2019), cf. Section 5.3

5.3 Verification

The model is verified against observed water levels at 5 locations and current speed and direction at 1 location.

5.3.1 Water level

As the model boundary is located where the North Sea meets the Atlantic Ocean, the simulated mean sea water level reference is the Atlantic Ocean.

Observed and simulated water levels in Ystad, Kalmar, Visby, Ronne and Gedser have been used as a reference for the comparison of observed and modelled water levels. The 5 locations of evaluation are shown in Figure 5.3.

Figure 5.3: Locations of evaluation regarding water levels. Locations are Gedser, Ystad, Ronne, Kalmar and Visby.

The time series comparison between observed and simulated water levels at the five locations are shown in Figure 5.4, Figure 5.5 and Figure 5.6 and qualitatively in Table 5.1.

In general, a reasonably good agreement between the observed and simulated water level is seen with a correlation coefficient higher than 0.92, where 1 is 100 % agreement.

Moreover, the exact location of the gauges in Gedser, Ystad, Ronne, Kalmar and Visby, is unknown, thus local effects are not included in the simulated water levels.

When comparing the water level in Figure 5.4, Figure 5.5 and Figure 5.6 is it important to have in mind that the simulated water level is according to the mean water level in the Atlantic Ocean which is different from the Swedish mean level RH 2000.

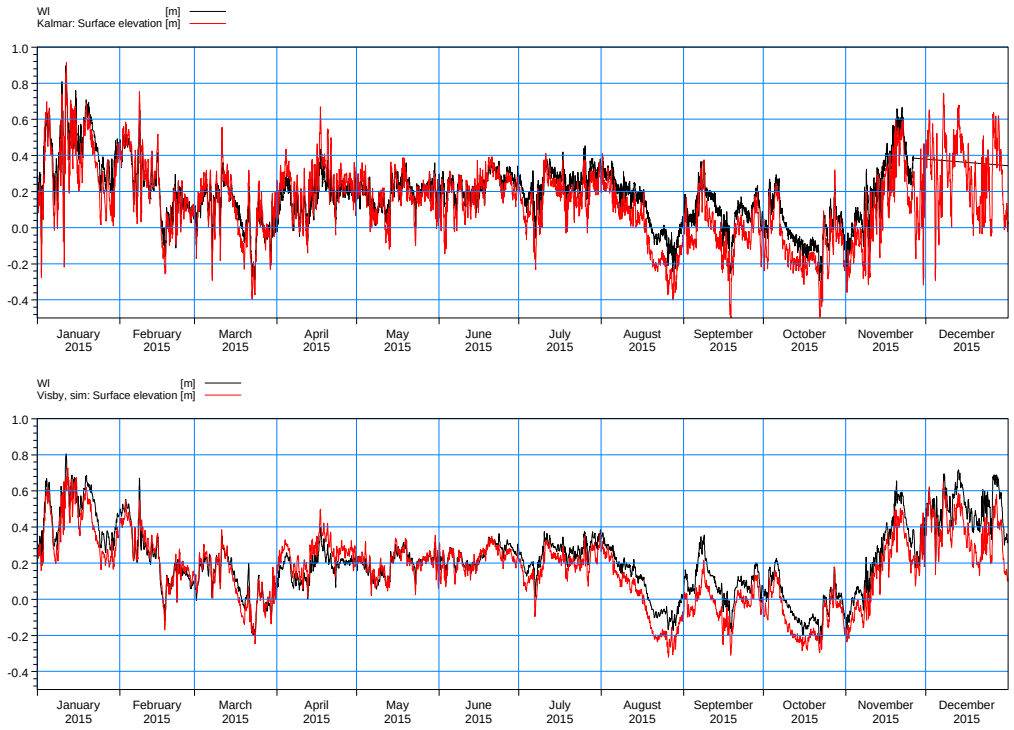

Figure 5.4: Top: Kalmar, bottom: Visby – Comparison of observed (black) and simulated (red) water level.

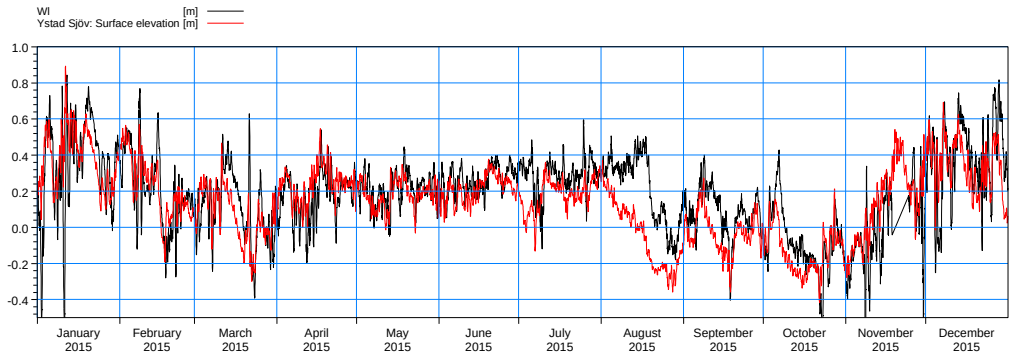

Figure 5.5: Ystad – Comparison of observed (black) and simulated (red) water level.

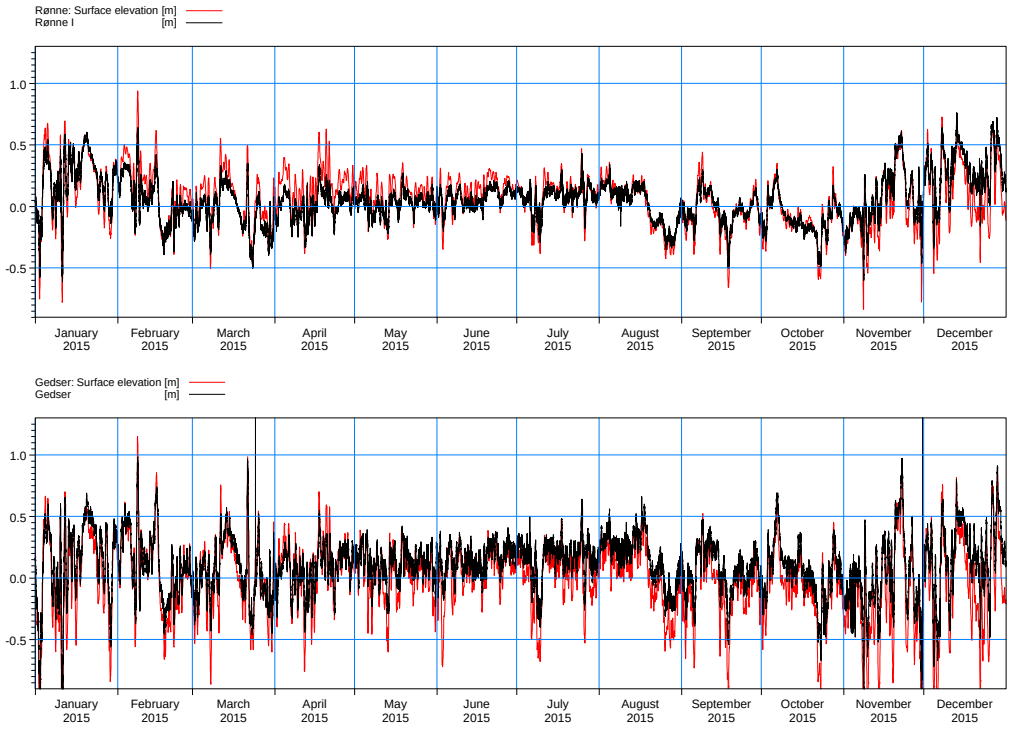

Figure 5.6: Top: Ronne, bottom: Gedser – Comparison of observed (black) and simulated (red) water level.

Table 5.1: Quality Index, observed versus simulated water level in Ystad, Kalmar and Visby

Quality index, description	Abbreviation	Unit	Ystad	Kalmar	Visby
Mean difference	BIAS	[m]	0.07	0.06	0.01
Absolute mean difference	AME	[m]	0.12	0.09	0.07
Root mean square	RMSE	[m]	0.15	0.12	0.08
Correlation coefficient	CC	[-]	0.92	0.94	0.96

5.3.2 Current

For verification of the hydrodynamic model observed and simulated current speed and directions from the At the MARNET buoy Arkona Basin have been compared and found to have an acceptable agreement, Figure 5.7.

Data from the buoy are shown as:

- "Depth Avg.": an average for all the data except for the data at 4 m;
- "Avg. 8-16m": an average over data between 8 and 16 m i.e. top layer and
- "Avg. 36-42": an average over data between 36 and 42 m i.e. bottom layer.

The modelled current is a depth average.

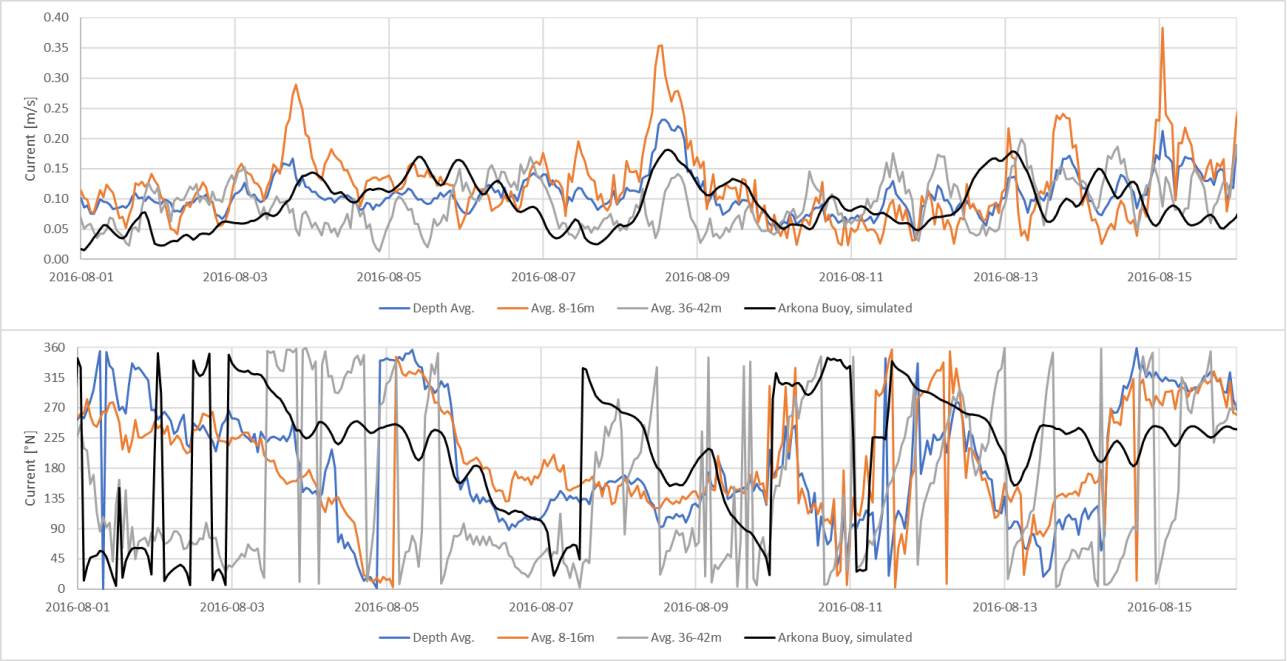

Figure 5.7: Arkona Buoy, Comparison of observed and simulated current speed (Top) and direction (Bottom).

5.4 Selection of simulation period

The simulation period for the installation activities across the whole wind farm is selected to cover the calmest period of the year based on the assumption that when the current or movement of the sediment is at the lowest the concentration and also the sedimentation will be at the highest. Anyway, due to the length of the installation period, it covers both periods in the summer and winter.

The general current pattern is dominated by a westerly current, probably driven by the dominating westerly wind, Figure 5.7.

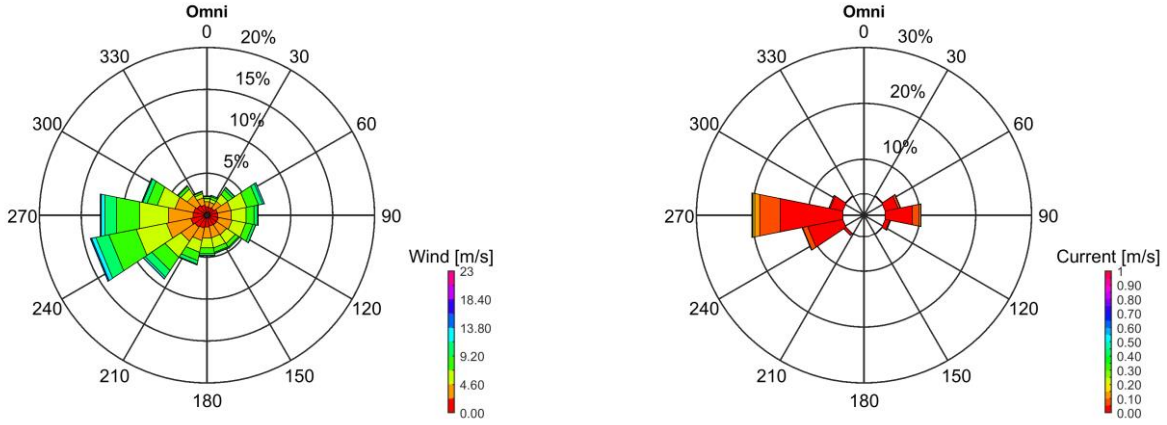

Figure 5.8: Wind (left) and current (right) rose for the year 2008 to 2018 at the centre of the wind farm.

The current speed is for more than 90% of the time, less than 10 cm/s and only for around 0.6% above 20 cm/s. The simulated water level and current are shown in Figure 5.8. The few situations with currents above 20 cm/s all seem to happen in the winter period.

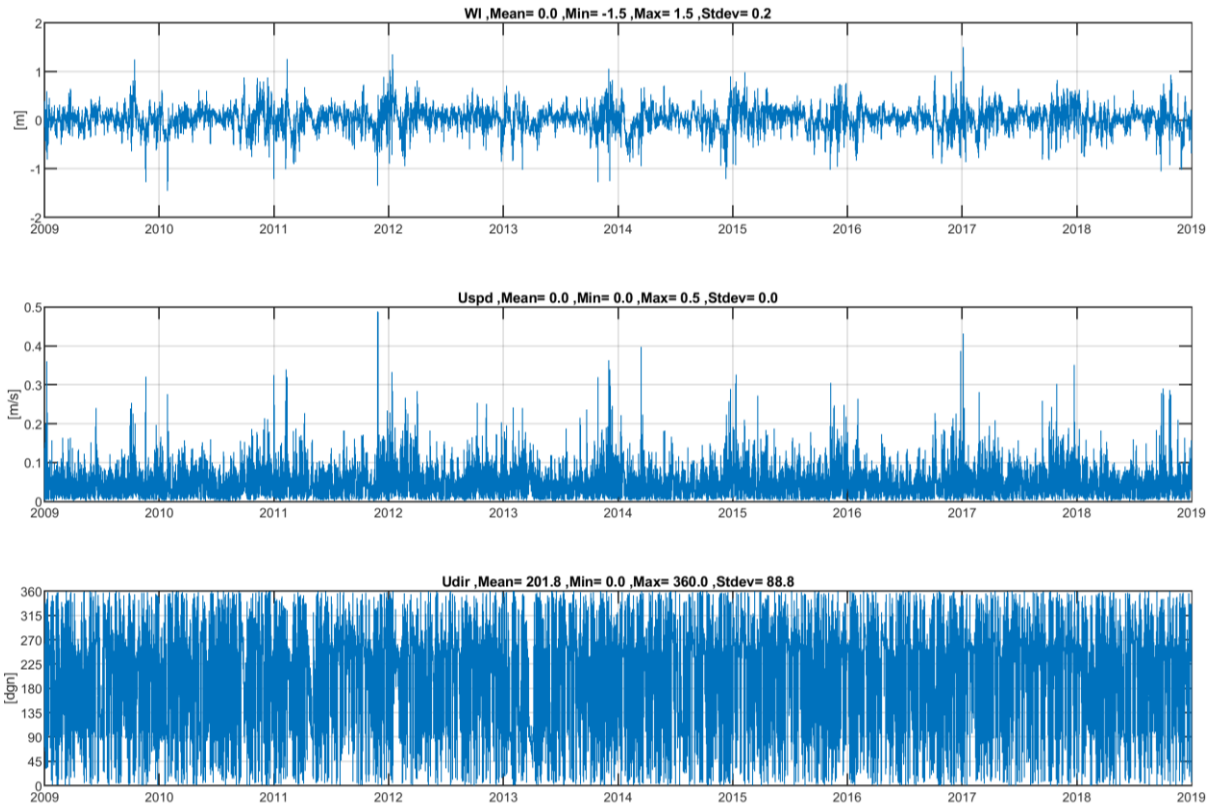

Figure 5.9: Water level, current speed and current direction at the centre of the wind farm from 2008 to 2018.

The year with the wind/current conditions closet the average is found to be 2010, cf. Appendix 1, Appendix 2 and Appendix 3.

5.5 Foundations – blocking

Current and waves are driven by differences in impact, wind and tide. The establishment of a wind farm will increase the hydraulic resistance which, potentially, may change both the water exchange, current and wave pattern.

The impact on current and waves comes partly from a direct blockage given by the wind turbine foundations as well as from a downstream reduction of the local wind as a result of the energy the wind turbines take out of the wind.

The reduction from the foundations is entered both in the hydrodynamic model and in the wave model as point structures corresponding to the location of the foundations with information regarding the dimension and design of the foundation. In the model, this is expressed by an increased hydraulic resistance/reflection in the calculation cells (DHI, u.d.) where the wind turbine foundations are located.

5.6 Wind reduction

The regional impact is not only due to the presence of the foundations but also because of the reduction in the wind downstream of the wind farm.

To reduce the downstream wind, a method described in (Erik Damgaard Christensen, Sten Kristensen & Rolf Deigaard, 2014) has been used, where the wind is reduced concerning the width and length that the park has for the wind direction in question as a function of the distance to the park. The reduction factor has been found for angles of 15°, which are subsequently applied to the time series of wind field on an hourly basis.

6 CFD model, description and setup

To model the mixing of layers in the water column distinguished by different salinities (densities), a numerical model is set up using the open-source library OpenFOAM (Open Field Operation And Manipulation (OpenFOAM, u.d.)).

OpenFOAM solves the Navier Stokes Equations on a domain (cell level) discretized to a level allowing for relatively fast computation and reasonable accuracy.

6.1 Model setup

6.1.1 Model mesh

To contain the foundation structure a 650 m long (-150 to +500 m), 200 m (+/ 100 m) wide and 45 m high (the water depth) flume is established, with the foundations located in (x,y)=(0,0). The largest cells are 1x1x1 m at the inlet/outlet and down to a minimum of 0.25 m close to the structure. An example of the entire model domain, including a substructure is shown in Figure 6.1.

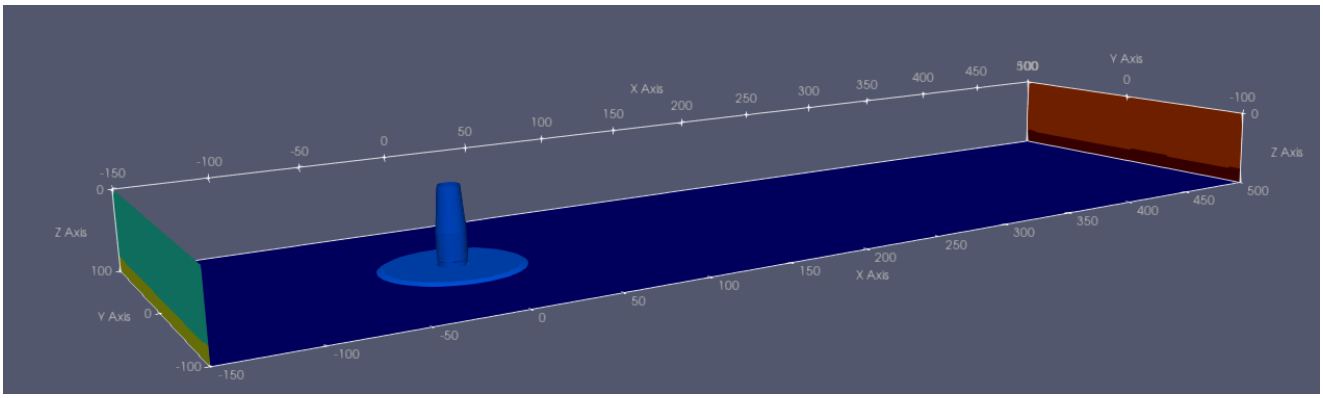

Figure 6.1: Computational mesh – example; Green & Light Green: inlet (left), Red & Dark Red: outlet (right), Blue: bottom and Light Blue: MP+scour protection.

6.1.2 CFD model parameters

Boundary conditions are applied through the Waves2Foam library which is based on OpenFOAM. OpenFOAM solves the equations for fluid impact, velocity, volume fraction and turbulence (described by a turbulence model) for each cell in the model domain.

The hydrodynamic parameters to be calculated are:

- Ux, Uy, Uz : the velocity [m/s];
- p : total impact [N/m2] given as p = p_h + p_rgh = ρg(η - y);
- p_rgh : the 'dynamic impact' [N/m2], pseudo impact and has no physical meaning (=ρgη) ;
- alpha.salt : the volume fraction of saline water (in a cell) [-].

To obtain a reasonable calculation time and accuracy of the results, turbulence is modelled (i.e. not solved on cell level) through the k-ω SST formulation to obtain:

- k: turbulence kinetic energy;
- ω: dissipation rate;
- nut: turbulence viscosity;

The shear stress transport (SST) formulation combines the best of two worlds using the k-ω formulation in the inner parts of the boundary layer and switching to a k-w behaviour in the free-stream.

Two phases are defined for the flow in the model. One phase is for the water in the top layer and one for the water in the bottom layer. The distinction between the two phases is defined by a parameter alpha which for the water at the bottom layer is 1 and the top layer 0. Hence, alpha varies between 0 and 1 depending on how large a fraction of each cell is in the bottom layer or top layer.

6.1.3 Inlet boundary

To the left in Figure 6.1, the incoming flow) divided into a top and bottom layer defined by the water depth of the pycnocline.

The top and bottom part of the inlet is specified, allowing for a specification of exact values for the velocity as well as the density on the boundaries, known as a Dirichlet condition. The free stream velocity is set to e.g. 0.3 m/s for the top and e.g. 0.1 m/s for the bottom. For the "upper" and "lower" part of the water column, the density is set to e.g. 1005 kg/m^3 and e.g. 1015 kg/m^3 respectively.

6.1.4 Outlet boundary

The outlet is defined with the same top and bottom layer as the inlet but with the boundary described by the model i.e. a Neumann boundary; the gradient is constant and will not influence the model.

6.1.5 Seabed and structure – wall conditions

The seabed and the surface of the structure are treated as solid walls with a roughness $K_s = 2.5 \times d$ where d is the average grain diameter and K_s the roughness constant. For the sandy seabed, $K_s = 5 \times 10^{-4}$ and for the concrete structure $K_s = 2.5 \times 10^{-3}$.

To avoid influence from the two parallel sides (of the domain) the velocities were specified as type symmetry.

The impact at the seabed and the structure is defined as a Neumann condition, i.e. no change in the impact at the boundary and formulated as dp/dy=0.

7 Impact, General Hydrodynamics

The impact due to the planned wind farm starts with a presentation of the present conditions followed by a presentation of the estimated changes given by the establishment of the planned wind farm with 129 25 MW GBS. Both in numbers and dimensionwise a setup likely to be very conservative i.e. the estimated impact is expected to be higher than for the build wind farm.

The following is a general description of the current, wave, shear stress and flow conditions (baseline) compared to the situation with the planned wind farm consisting of 129 25 MW GBS. The results are for each parameter illustrated for the present conditions and the relative changes caused by the wind farm.

7.1 Current

The annual average current speeds inside the local model domain are shown in Figure 7.1 (top) for the baseline case. In the eastern part of the wind farm, the current speed is slightly larger compared to the remainder of the wind farm. When the 129 GBS foundations are installed, these slightly larger current speeds cause a larger impact in the eastern part of the wind farm, as seen at the bottom of Figure 7.1 leading to reduced average annual speeds across the entire wind farm.

The largest reduction in these annual average current speeds ranges to 5 mm/s (0.005 m/s) extending up to approx. +/-125 m from the foundations in the eastern part of the wind farm and the dominating current directions (see Figure 5.7). Reduced current speeds caused by the presence of the wind farm seems to propagate towards the southwest in the mean current direction.

In terms of the distribution of the annual maximum current speed inside the wind farm, the same tendency is found for the annual average, i.e. largest drop in maximum current speeds in the eastern part of the wind farm, Figure 7.2 top. The area with the largest decrease propagates downstream of the wind turbines leaving trails with small increases in the annual maximum current speed in between the foundations.

The largest decrease in the maximum current speed ranges to approximately 2 cm/s (0.02 m/s) whereas the largest increase is somewhere between 1 cm/s-2 cm/s. The latter occurs inside as well as outside the wind farm, although the pattern of the decreased annual maximum current speed does not follow the mean current direction to the same extent as inside the wind farm.

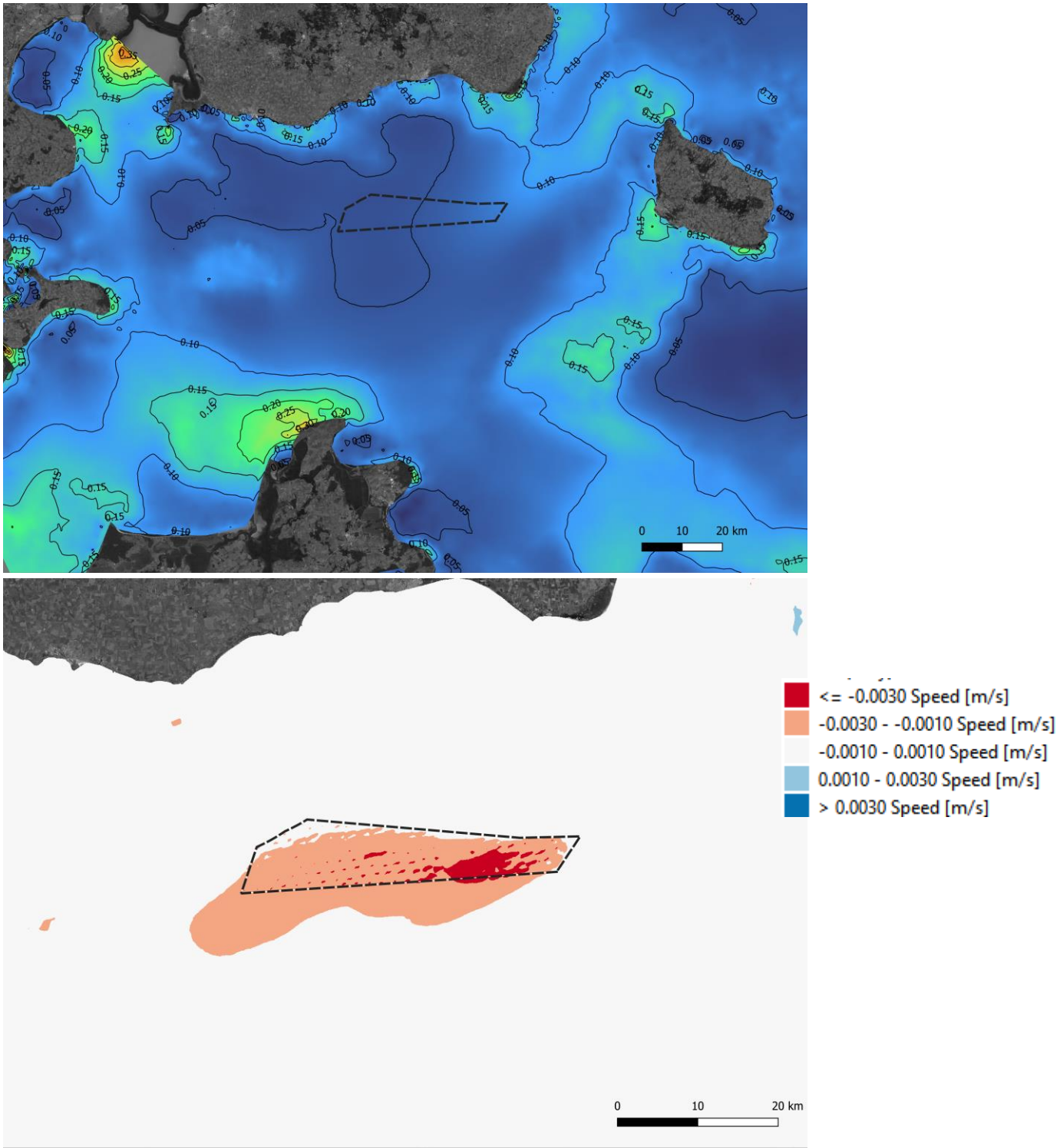

Figure 7.1: Average current speed year 2016. Top: average current speed [m/s], Bottom: impact due to 129 GBS

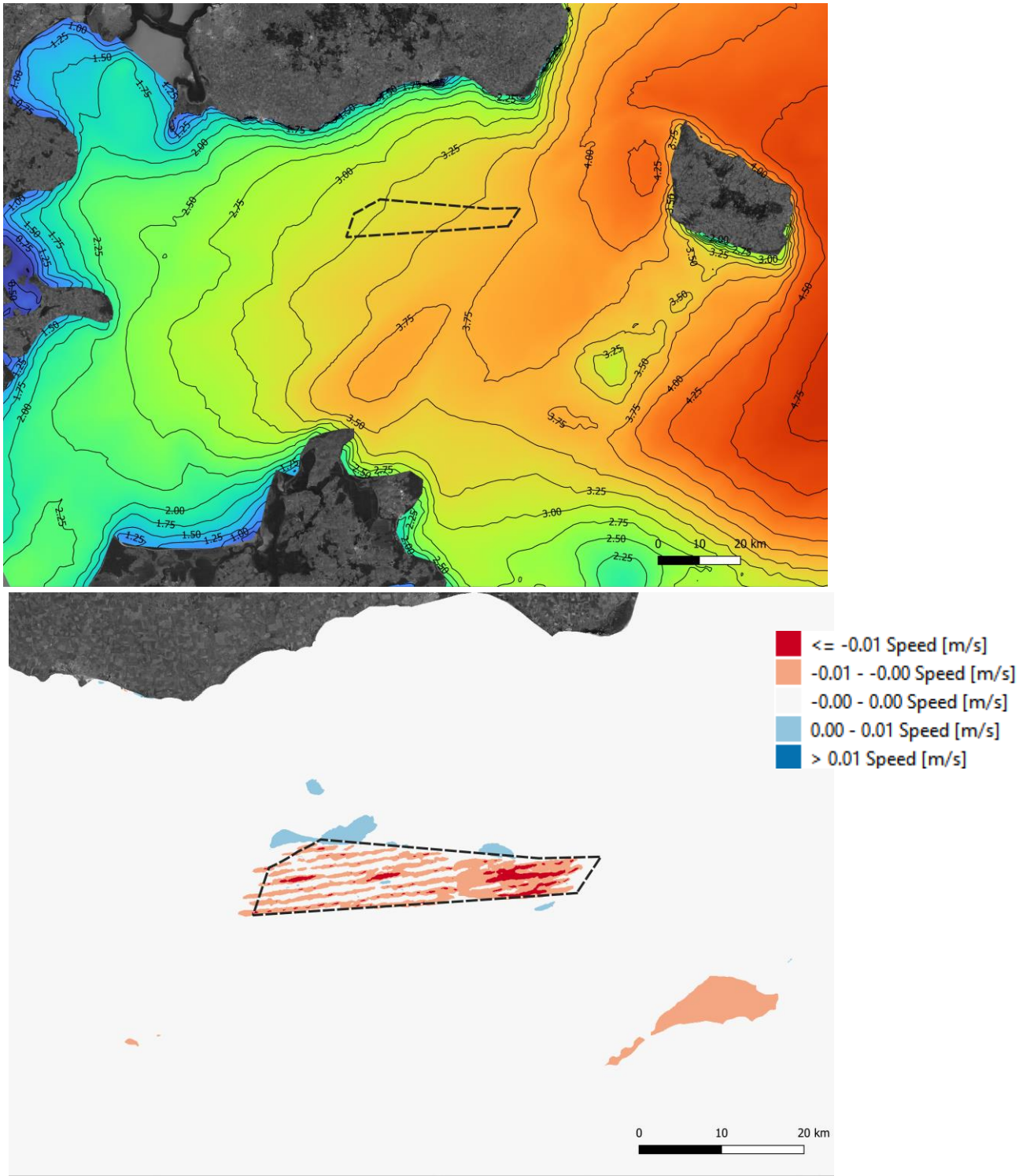

Figure 7.2: Maximum current speed year 2016. Top: maximum current speed [m/s], Bottom: impact due to 129 GBS

7.2 Waves

The impact on both the average and maximum significant wave height is limited as shown in Figure 7.3 and Figure 7.4 respectively.

For the average significant wave height, the eastern half of the wind farm area is influenced by wave heights between 0.8 m and 0.9 m whereas the western half experiences average wave heights between 0.7 m and 0.8 m, Figure 7.3 top.

The effect of having installed all wind turbine foundations is that the average wave height is increased by less than 1 cm across the entire wind farm as seen at the bottom of Figure 7.3. The layout of the wind turbines is vaguely outlined, which means the change is practically zero.

Figure 7.4 shows the change in maximum wave heights caused by the presence of the wind turbine foundations. In the top of Figure 7.4, it is seen that the maximum wave heights without the presence of the foundations vary between 3.25 m and almost 3.75 m, increasing from west to east.

The effect of the foundations is split into a western and eastern half of the wind farm area. On the western side, the maximum significant wave heights increase by up to 1 cm as seen at the bottom of Figure 7.4. A decrease is seen for the eastern half also reaching a maximum of approximately 1 cm. The magnitude of the change is in both cases practically negligible.

The largest change in the maximum wave heights is seen at the Swedish shorelines (Skåne) which are most likely due to the location of where the waves are breaking. A change in water level at shallow waters make waves break at different locations which most likely is the effect shown in Figure 7.4

This is the same reason why there is a small impact on both the average and maximum waves in a distance to the wind farm.

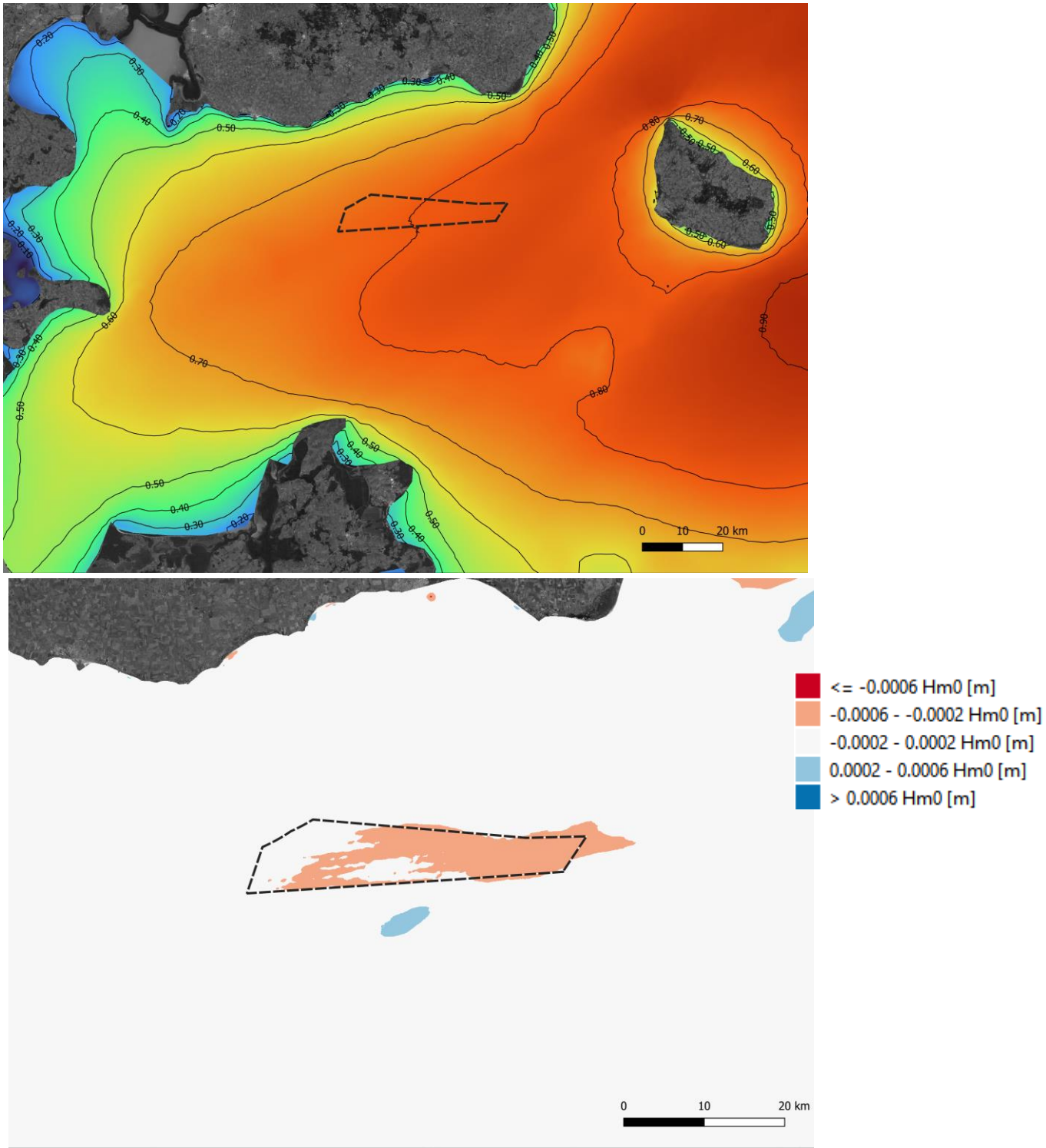

Figure 7.3: Average H_{m0} year 2016. Top: average H_{m0} [m], Bottom: impact due to 129 GBS

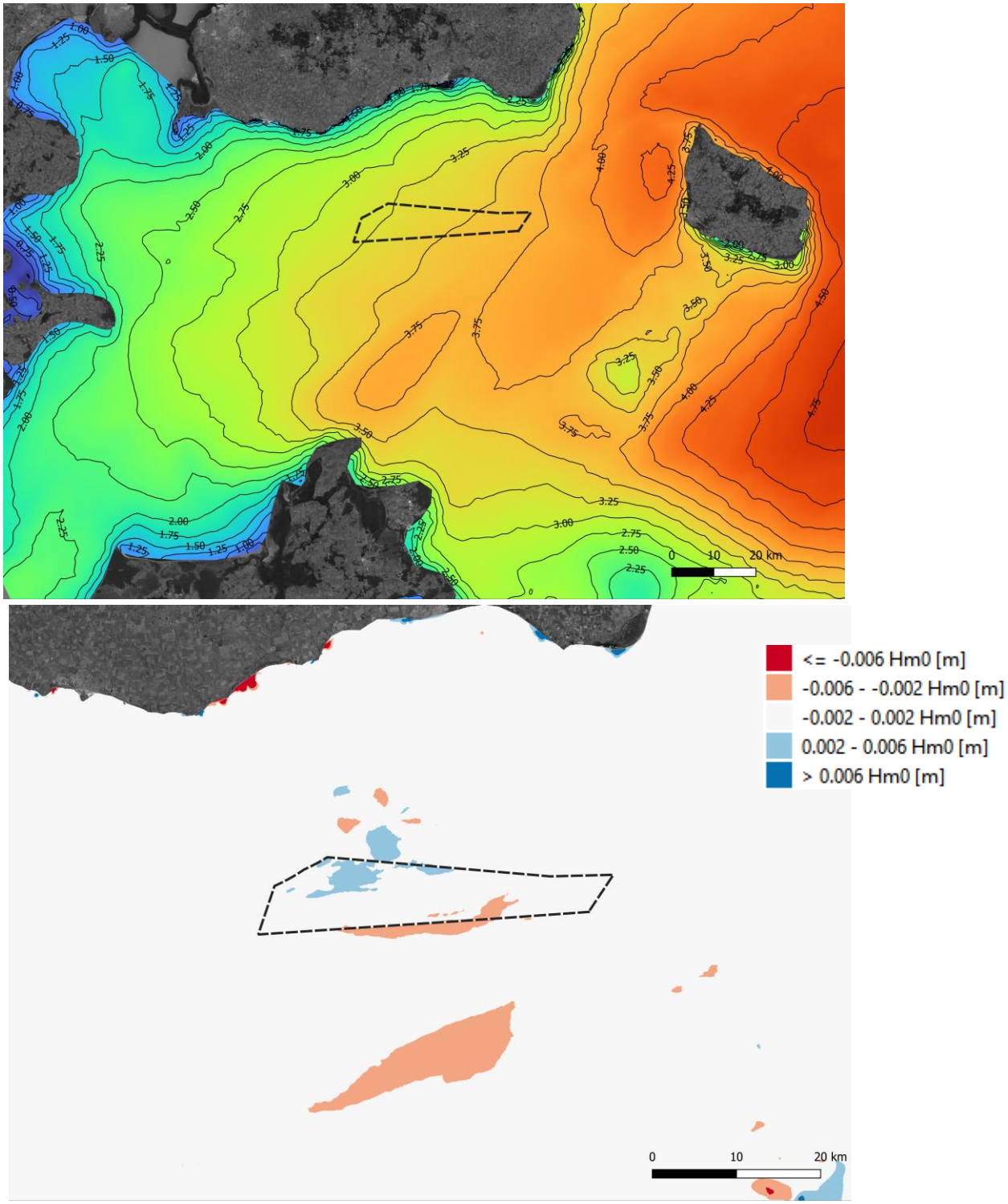

Figure 7.4: Maximum H_{m0} year 2016. Top: maximum H_{m0} [m], Bottom: impact due to 129 GBS

7.3 Shear Stresses

The contour of bed shear stresses before installation of the wind turbine foundations are very similar to the contour of current speeds, as the bed shear stress is directly proportional to the current speed. Consequently, the average annual bed shear stress across the entire wind farm varies between 0 N/m^2 and 0.01 N/m^2 as shown at the top of Figure 7.5. This is a small number and is aligned with sediment classification made SGU i.e. Mud.

The largest change in the average bed shear stresses occurs inside the wind farm footprint and is primarily increased by up to 0.001 N/m^2 indicating a decrease when the current speed decrease.

The similarity between average bed shear stress and the current speed is also seen when comparing the maximum annual bed shear stresses to current speeds at the top of Figure 7.6. The bed shear stress without the wind farm present increase from 0.1 N/m^2 ranges between 0.1 and 0.25 N/m^2, increasing from the west to east.

In the eastern part of the wind farm, the bed shear stresses change the most, as a decrease up to approximately 0.01 N/m^2 is experienced. There are some small patches in between foundations with increased bed shear stresses, which is also aligned with the increase in current speeds at the same locations.

Outside the western part of the wind farm, the reduced bed shear stresses extend beyond the wind farm footprint, and immediately north hereof a patch is found with increased bed shear stresses.

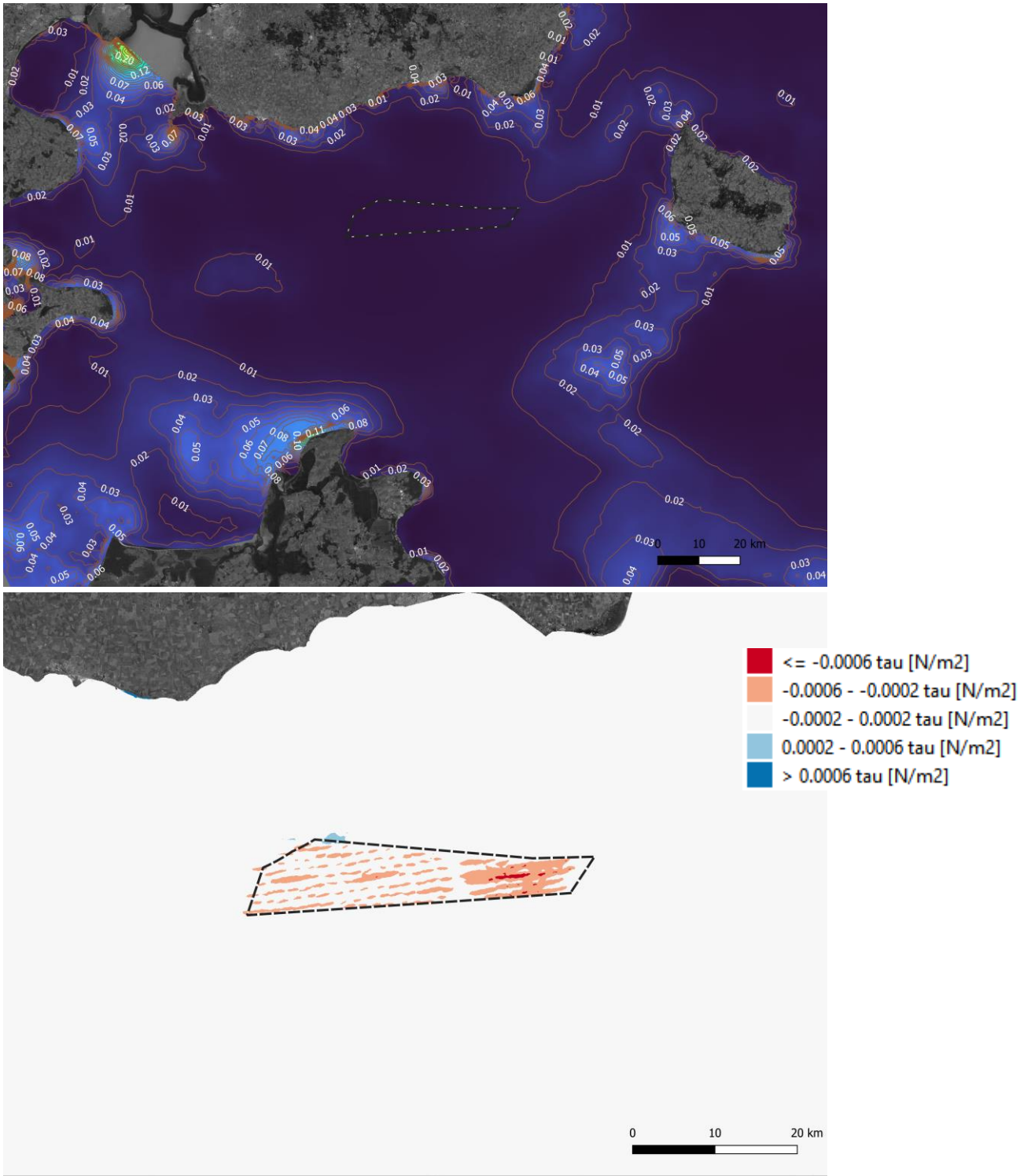

Figure 7.5: Average shear stresses in the year 2016. Top: average shear stress [N/m²], Bottom: impact due to 129 GBS

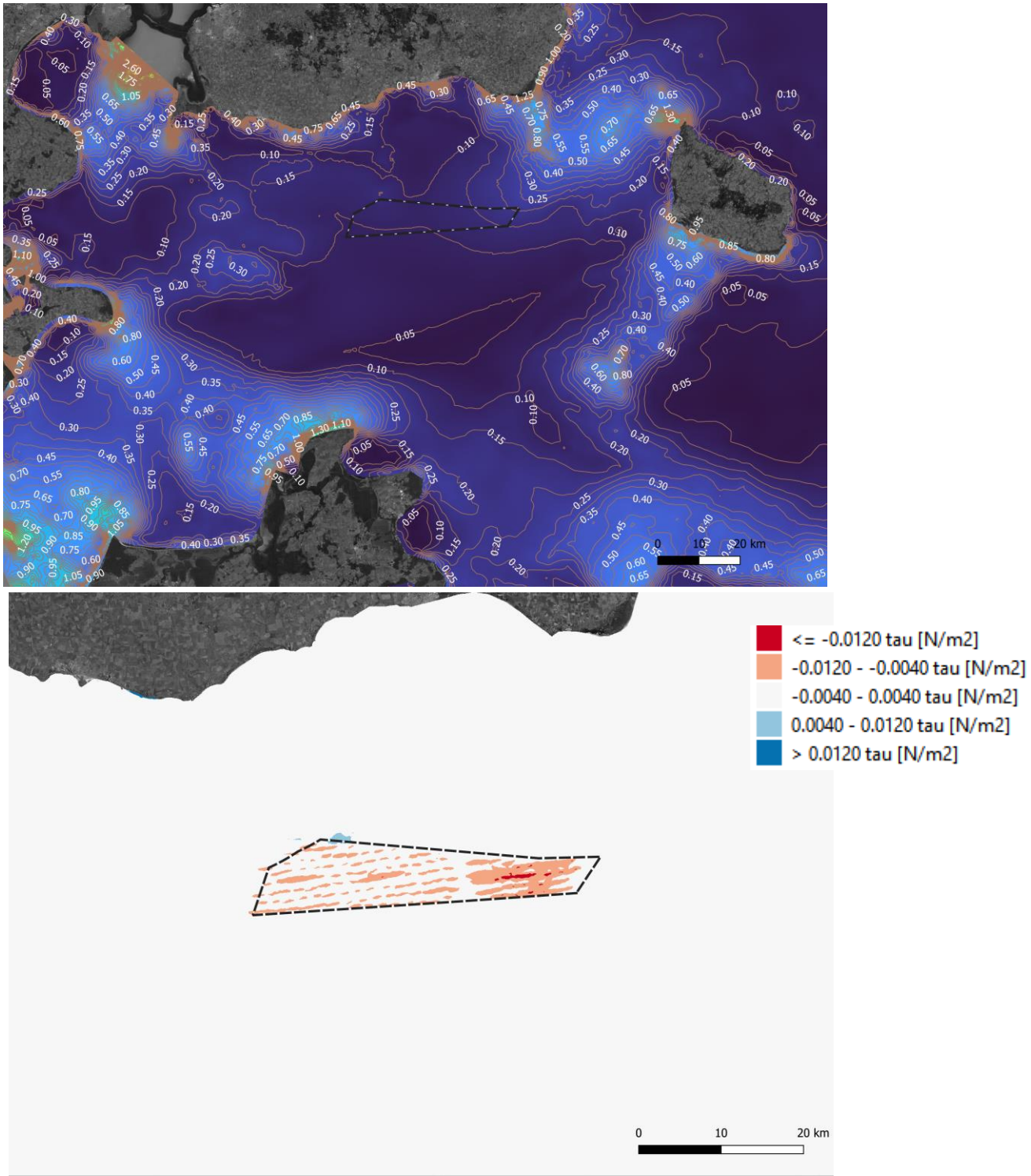

Figure 7.6: Maximum shear stresses in the year 2016. Top: maximum shear stress [N/m²], Bottom: impact due to 129 GBS

To assess whatever the change in the bed shear stresses may cause changes in the sediment transport, Figure 7.7 shows the correlation between the percentage in grain distribution and expected critical shear stress (the latter is the threshold which when exceeded indicates a movement of sediments).

In (NIRAS A/S, 2021), the sediment material assumed to dominate the seabed at the Triton OWF, is represented Figure 5.6 and Table 5.3. The seabed sediment is by (SGU, 2020) described as Mud which is interpreted as soft sediment with a high content of clay and silt e.g. a mixture of clay/silt and coarse silt plus sand; ration 18% clay and fine silt else coarser. According to Figure 7.7, this reveals critical shear stresses between 0.03 and 3 N/m^2 which has to be exceeded before a sediment transport may be initiated, the bed shear stress needs to be equal to or exceed the critical shear stress.

Particle classification name	Ranges of particle diameters φ	mm	Shields parameter (dimensionless)	Critical bed shear stress (τ_c) (N/m^2)
Coarse cobble	-7 – -8	128 – 256	0.054 – 0.054	112 – 223
Fine cobble	-6 – -7	64 – 128	0.052 – 0.054	53.8 – 112
Very coarse gravel	-5 – -6	32 – 64	0.05 – 0.052	25.9 – 53.8
Coarse gravel	-4 – -5	16 – 32	0.047 – 0.05	12.2 – 25.9
Medium gravel	-3 – -4	8 – 16	0.044 – 0.047	5.7 – 12.2
Fine gravel	-2 – -3	4 – 8	0.042 – 0.044	2.7 – 5.7
Very fine gravel	-1 – -2	2 – 4	0.039 – 0.042	1.3 – 2.7
Very coarse sand	0 – -1	1 – 2	0.029 – 0.039	0.47 – 1.3
Coarse sand	1 – 0	0.5 – 1	0.033 – 0.029	0.27 – 0.47
Medium sand	2 – 1	0.25 – 0.5	0.048 – 0.033	0.194 – 0.27
Fine sand	3 – 2	0.125 – 0.25	0.072 – 0.048	0.145 – 0.194
Very fine sand	4 – 3	0.0625 – 0.125	0.109 – 0.072	0.110 – 0.145
Coarse silt	5 – 4	0.0310 – 0.0625	0.165 – 0.109	0.0826 – 0.110
Medium silt	6 – 5	0.0156 – 0.0310	0.25 – 0.165	0.0630 – 0.0826
Fine silt	7 – 6	0.0078 – 0.0156	0.3 – 0.25	0.0378 – 0.0630

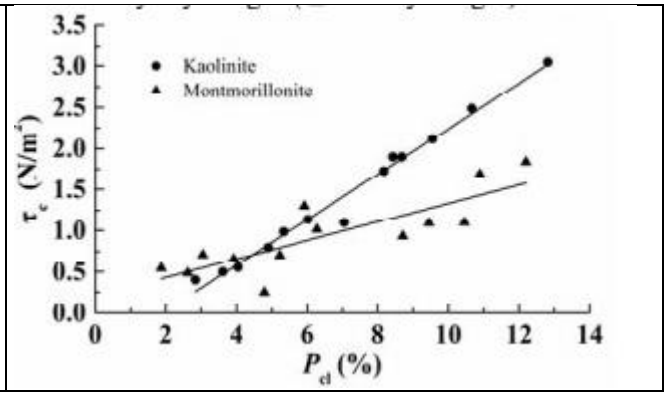

Figure 7.7: Left: critical shear stress as a function of grain diameter (U.S. Department of the Interior & U.S. Geological Survey, 2013); Right: critical shear stress as contents of clay (Fei-dong Zheng and Jian-feng, 2017) where P_{cl} is the percentage of clay contents and τ_c the critical shear stress.

As seen in Figure 7.5 and Figure 7.6 the bed shear stresses without the presence of the wind farm is approximately 0.01 N/m^2 and 0.25 N/m^2 on average and maximum results. The presence of the wind farm is most critical when looking at the maximum bed shear stresses, and with a potential increase of 0.01 N/m^2, it is highly unlikely that the presence of the wind farm will lead to further transport of sediment when constructed.

Development of scour pits close to the foundations has not been considered but could potentially lower the seabed to 1.3 times the pile diameter to a distance of 3 to 5 times the depth of the scour pit with the eroded material deposit downstream.

7.4 Flux, Local

The presence of a wind farm can cause blocking locally as well as on a larger scale, e.g. regionally. Therefore, a mass balance has been made to keep track of the flux across the borders of the wind farm.

For each of the four quarters of the year and the entire year, the sum of m^3 moving across the borders with and without the wind farm present have been modelled. The total sum for each period is compared to the sum for the baseline and reported in Table 7.1 as both m^3 and percentages.

Table 7.1: Flux across four borders of Triton Offshore Wind Farm

Period	Flux (+=in, -=out)		Flux (Baseline-GBS)	
	Baseline sum [m^3]	GBS sum [m^3]	Difference sum [m^3]	Difference [%]
Q1	3.49E+08	3.49E+08	-5.10E+04	0.01%
Q2	-4.09E+07	-4.08E+07	-3.82E+04	-0.09%
Q3	-2.51E+08	-2.51E+08	-8.70E+04	-0.03%
Q4	-1.34E+08	-1.34E+08	-1.37E+05	-0.10%
Year	-7.41E+07	-7.39E+07	-2.19E+05	-0.30%

The "Difference sum" is "Baseline" minus "GBS" where "Difference" is the changes in the flux caused by the 129 GBS e.g. a negative "Difference" means that the GBS reduce the total flux to the surrounding box.

As an example, over the entire year when the gravity-based substructures are installed, it is expected that the flux across the surrounding box will decrease by 0.30 %.

7.5 Summary, General Hydrodynamic

The Triton OWF gives raise to a local hydrodynamic blockage, and cause a reduction of current speed, wave heights as well as bed shear stress inside the wind farm area.

The changes in significant wave height, both on average and the maximum wave heights, are in practical terms negligible as they all are subject to +/-1 cm change due to the presence of the wind farm. Considering the sizes of the waves (0.8 m and 3.75 m for average and maximum wave heights) this change seems even more insignificant.

The current field and magnitude are subject to changes due to the installation of the wind turbines. The current speeds are reduced mostly on the eastern side of the wind farm and increased slightly north of the wind farm. Together with the local flux analysis, this indicates that the presence of the wind farm cause the flow (travelling in a south-western direction) to deviate slightly and propagate more towards west and south respectively.

The bed shear stress field changes in the same way as the current field. As these are directly proportional to one another, the bed shear stress decrease where the blockage is largest and increase in between the foundations as the current speed increase here too.
The changes in the bed shear stresses are quite unlikely to cause an excess of sediment transport, as the (assumed) critical shear stress in the area does not seem to be exceeded due to the presence of the wind farm. Except for speed up effects just next to the substructure which without mitigations is likely to generate local scour with a depth of 1.3 times the pile diameter to a distance of 3 to 5 times the depth of the scour pit.

8 Impact, Stratification

8.1 Stratification events, statistical analyses

The daily variation in the salinity for the measured depths are presented in Table 8.3. For the depths 2 to 7 m the daily variation is less than 0.2 PSU for 64% of the time whereas the same only is the case for 2.6% at 40 m water depth.

A similar picture is observed on the yearly variation. For down to 7 m the yearly variation is less than 5 PSU, increasing to 10 PSU at 16 m and 16 PSU below 40 m, Figure 8.1.

This indicates a reasonable stable top layer down to 7 m whereafter the variations in the salinity increase probably due to mixing, an inflow of more saline water from Kattegat or changes in the location of the stratification (halocline) due to e.g. wind setup in the Balti Sea (tilting the interface).

Table 8.3: [Text] Daily variation in the salinity presented as the difference of daily maximum and minimum.

Max-Min [PSU]		Water Depth [m]							
From	To	2	5	7	16	25	33	40	43
0.0	0.2	65.9%	65.3%	64.1%	50.4%	22.9%	6.0%	2.6%	5.7%
0.2	0.4	22.7%	23.1%	23.5%	26.1%	20.7%	8.8%	7.3%	10.1%
0.4	0.6	5.9%	6.0%	6.6%	10.3%	13.3%	12.7%	11.0%	12.9%
0.6	0.8	2.6%	2.4%	2.5%	3.8%	9.9%	13.3%	11.6%	11.0%
0.8	1.0	0.9%	1.2%	1.0%	2.4%	7.2%	12.5%	11.8%	11.2%
1.0	1.2	0.5%	0.8%	0.5%	1.8%	5.2%	9.3%	10.1%	7.1%
1.2	1.4	0.6%	0.4%	0.7%	1.5%	5.0%	9.1%	8.2%	6.8%
1.4	1.6	0.3%	0.3%	0.4%	0.5%	3.1%	6.6%	6.8%	6.2%
1.6	1.8	0.1%	0.1%	0.3%	0.3%	2.4%	4.7%	4.7%	4.6%
1.8	2.0	0.4%	0.3%	0.2%	0.8%	2.3%	3.2%	4.9%	3.9%
2.0	2.2	0.1%	0.1%	0.2%	0.3%	1.5%	2.9%	3.4%	2.8%
2.2	2.4	0.0%	0.1%	0.0%	0.0%	1.2%	2.1%	3.7%	2.8%
2.4	2.6	0.0%	0.0%	0.1%	0.3%	0.8%	1.5%	2.9%	2.2%
2.6	2.8	0.0%	0.0%	0.0%	0.3%	0.7%	1.0%	1.4%	1.9%
2.8	3.0	0.0%	0.0%	0.0%	0.2%	0.6%	1.4%	1.6%	1.7%
3.0	3.2	0.0%	0.0%	0.0%	0.1%	0.4%	0.7%	1.0%	1.2%
3.2	3.4	0.0%	0.0%	0.0%	0.3%	0.5%	0.6%	1.0%	0.9%
Sum		100.0%	100.0%	100.0%	100.0%	99.9%	99.9%	99.9%	100.0%

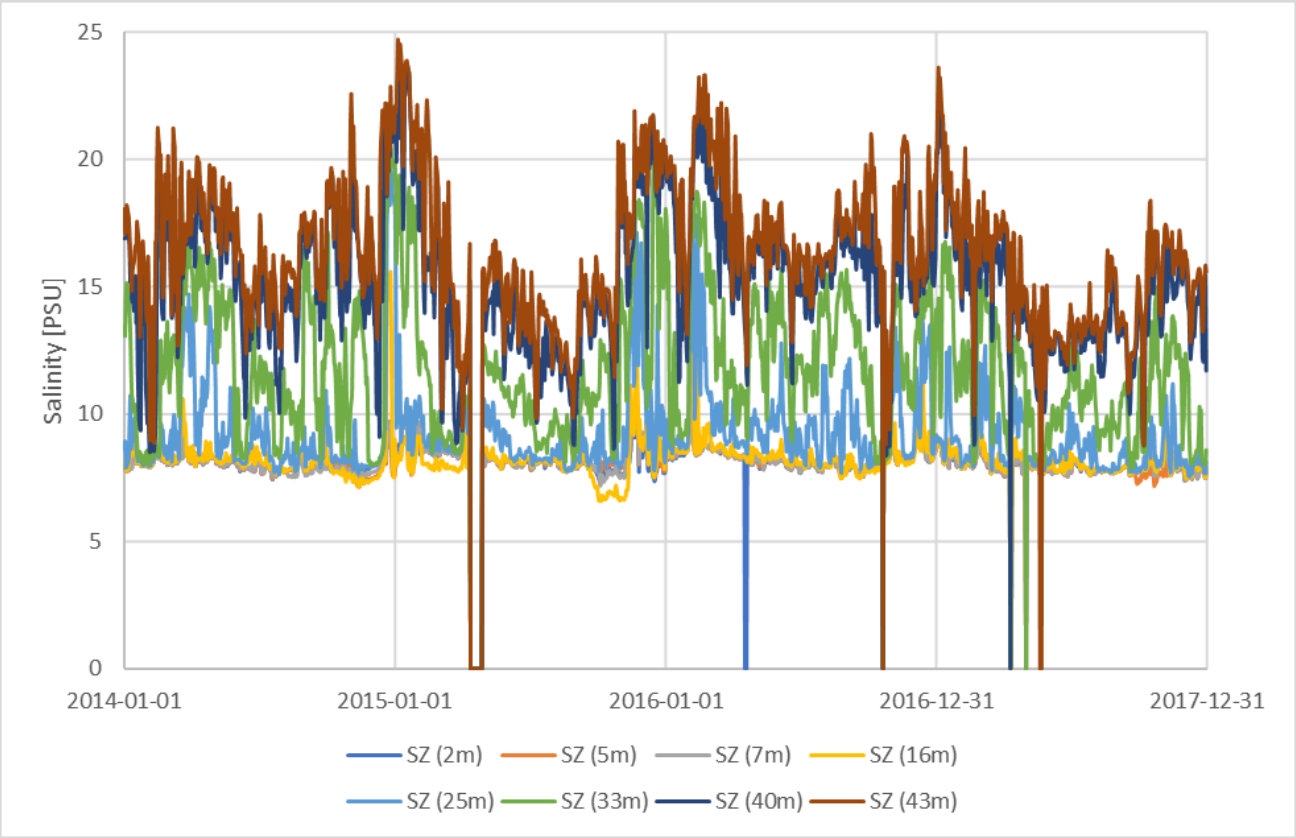

Figure 8.1: Daily average salinity for the measured water depths

For investigation of the impact on the stratification (mixing), the data set has been brought down to an affordable number of events given by current speed and current direction in the top and bottom layer vs. the depth of the pycnocline as described below:

1) Determination of the density based on the observed salinity and temperature (Arkona Buoy) per time step (hourly basis);
2) Identification of the pycnocline based on the largest gradient;
3) Determination of the average density in the top and bottom layer defined by the location of the pycnocline;
4) Determination of the average current speed and direction in the top and bottom layer;
5) Determination of the difference in the density as top layer vs. bottom layer - Δrho;
6) Determination of the difference between the current speed in the top layer vs. the bottom layer (to avoid influence from the wind data from 4 m was excluded) - ΔU;
7) Scatter table of ΔU vs. Δrho showing per cent of the time for selected intervals;
8) Scatter table of ΔU vs. Δrho showing the location of the halocline for a percentile of 25%, 50% and 75% for the same intervals as above.

The outcome of the analyses is presented in Table 8.1 as the per cent of the time for various combinations of differences in densities and current speed between the top and bottom layer e.g. the most common situation (16.1%)

is a difference in density between 4 to 6 kg/m^3 with a current speed 0.1 m/s higher in the top layer and the pycnocline located in -36.5 m.

Table 8.1: Difference in density (rho) vs. difference in current speed (top layer – bottom layer) – Top: per cent of the time, Bottom: location of the pycnocline found as the 50% percentile.

			Rho Difference [psu] (top-bottom)						
	From		0	2	4	6	8	10	Sum
		To	2	4	6	8	10	12	
Current Speed Difference [m/s] (+ => top layer highest, - => bot. layer highest)	-0.4	-0.3	0.0%	0.0%	0.0%	0.0%	0.0%	0.0%	0.0%
	-0.3	-0.2	0.0%	0.0%	0.1%	0.1%	0.0%	0.0%	0.3%
	-0.2	-0.1	0.1%	0.4%	1.1%	1.0%	0.4%	0.1%	3.0%
	-0.1	0.0	0.5%	2.4%	9.2%	6.6%	2.0%	0.3%	20.9%
	0.0	0.1	0.7%	4.4%	16.1%	14.6%	3.5%	0.8%	39.9%
	0.1	0.2	0.6%	2.3%	8.1%	12.2%	3.5%	0.6%	27.4%
	0.2	0.3	0.1%	0.5%	1.9%	2.9%	1.2%	0.2%	6.7%
	0.3	0.4	0.0%	0.0%	0.3%	0.4%	0.4%	0.1%	1.3%
	0.4	0.5	0.0%	0.0%	0.1%	0.1%	0.1%	0.0%	0.3%
	0.5	0.6	0.0%	0.0%	0.0%	0.0%	0.0%	0.0%	0.1%
Sum			1.9%	10.0%	37.0%	37.8%	11.2%	2.0%	100.0%

			Rho Difference [psu] (top-bottom)					
	From		0	2	4	6	8	10
		To	2	4	6	8	10	12
Current Speed Difference [m/s] (+ => top layer highest, - => bot. layer highest)	-0.4	-0.3	-	-	-36.5	-	-32.8	-36.5
	-0.3	-0.2	-	-32.8	-36.5	-29.0	-20.5	-29.0
	-0.2	-0.1	-20.5	-29.0	-36.5	-36.5	-36.5	-36.5
	-0.1	0.0	-20.5	-36.5	-36.5	-36.5	-36.5	-29.0
	0.0	0.1	-41.5	-36.5	-36.5	-36.5	-36.5	-36.5
	0.1	0.2	-41.5	-41.5	-41.5	-36.5	-41.5	-41.5
	0.2	0.3	-41.5	-41.5	-41.5	-41.5	-36.5	-36.5
	0.3	0.4	-	-41.5	-41.5	-41.5	-36.5	-41.5
	0.4	0.5	-	-	-41.5	-41.5	-41.5	-41.5
	0.5	0.6	-	-41.5	-41.5	-41.5	-41.5	-

Table 8.2: Selected events; 1: Blue, 2: Green, 3: Red, 4: Purple and 5: Black in Table 8.1, Top. "Time": per cent of the time, "Pycnocline": water depth, "rho, top": average density in the top layer, "rho, bot": average density in the bottom layer, "d rho": difference in density, "U, top": average current speed in the top layer and "U, bot": average current speed in the bottom layer.

Event	Duration, estimated	Pycnocline	rho, top	rho, bot	d rho	U, top	U, bot
	[%]	[m]	[kg/m^3]	[kg/m^3]	[kg/m^3]	[m/s]	[m/s]
1	35.1%	-36.5	1005	1013	8	0.2	0.1
2	32.2%	-41.5	1005	1009	4	0.2	0.1
3	8.4%	-40.0	1005	1012	7	0.4	0.1
4	2.9%	-29.0	1005	1012	7	0.1	-0.1
5	21.4%	-36.0	1005	1011	6	0.1	0.2

8.2 Worst-case substructure

For comparison of the impact due to the three types of foundations: gravity-based, jacket and monopile substructure a standard model of each type was created based on the dimensions for the primary structure.

The substructure causing the largest impact on the mixing is defined as the one increasing the density in the top layer the most. This is in the model determined as the substructure with the largest changes in the average density 450 m downstream after 4320 seconds.

Except for the water depth of the pycnocline is the input to test case listed in Table 8.3. For this case, the pycnocline is placed at -36 m.

Table 8.4: Input to the CFD to determine the substructure causing most mixing

	U	P	k	ω	Density
	[m/s]	[Pa]	[m^2/s^2]	[s^{-1}]	[kg/m^3]
Top Layer	0.3	-	0.05	-	1005
Bottom layer	0.1	-	0.05	-	1015

The changes in the density in the top layer (from 0 to -36 m) for the cases after 4320 seconds are

- Baseline: 4.45 % (background mixing)
- GBS: 4.46 %
- MP: 4.51 %
- Jacket: 4.45 %

The jacket is in line with the background mixing, the GBS increases the mixing by 0.01% and the MP by 0.06% thus the latter can be considered to be the one causing the largest impact.

The influence on the current for the 3 types of substructure is after 4320 seconds illustrated:

- MP: Figure 8.1, estimated eddy period 500 seconds;
- Jacket: Figure 8.2, estimated eddy period 160 seconds;
- GBS: Figure 8.3, estimated eddy period between 630 to 1600 seconds

The oscillation time (T) for the eddy is given by

$T=D/(U \cdot St)$, where

D is the diameter of the pile and St Strouhalt's number which in these cases are around 0.4

As listed above the time for the eddy to develop depends on, among other things, the diameter of the substructure which again on the amount of turbulence generated by the substructure.

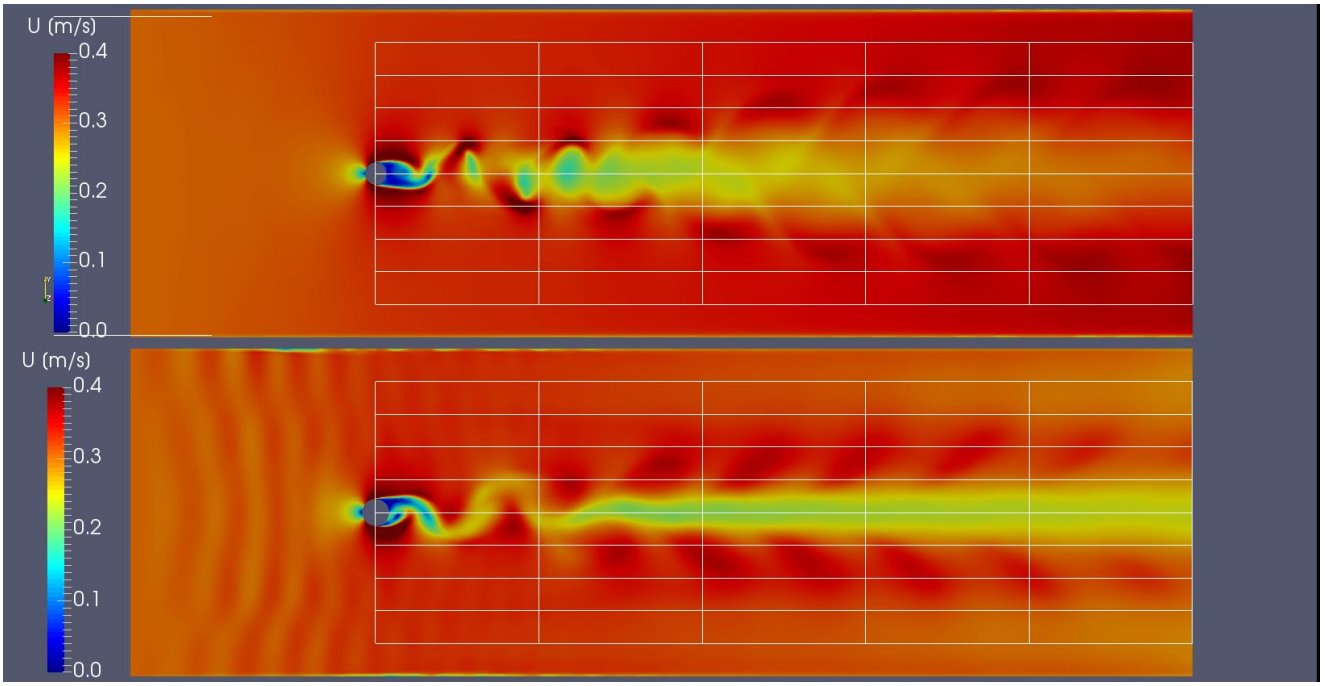

Figure 8.2: MP, current speed at -5 and -25 m (top and bottom) after 4320 s. The grid is 400 m long and +/-80 m wide

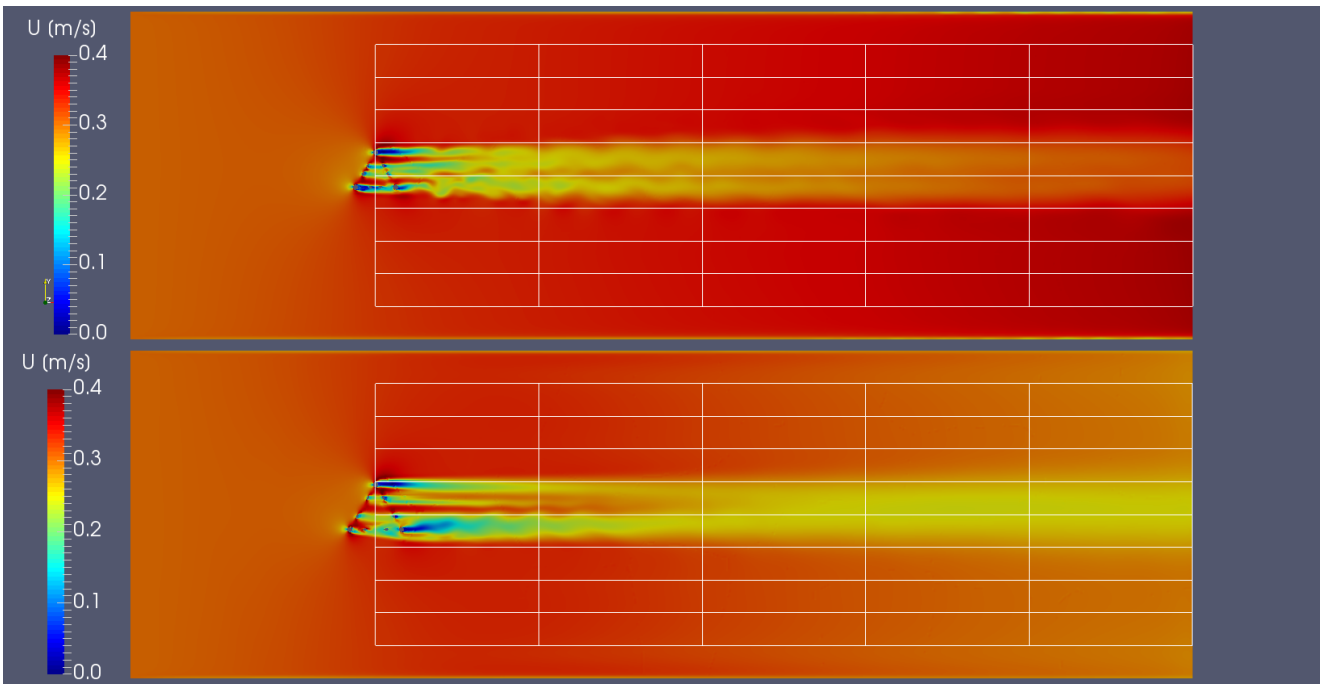

Figure 8.3: Jacket, current speed at -5 and -25 m (top and bottom) after 4320 s. The grid is 400 m long and +/-80 m wide.

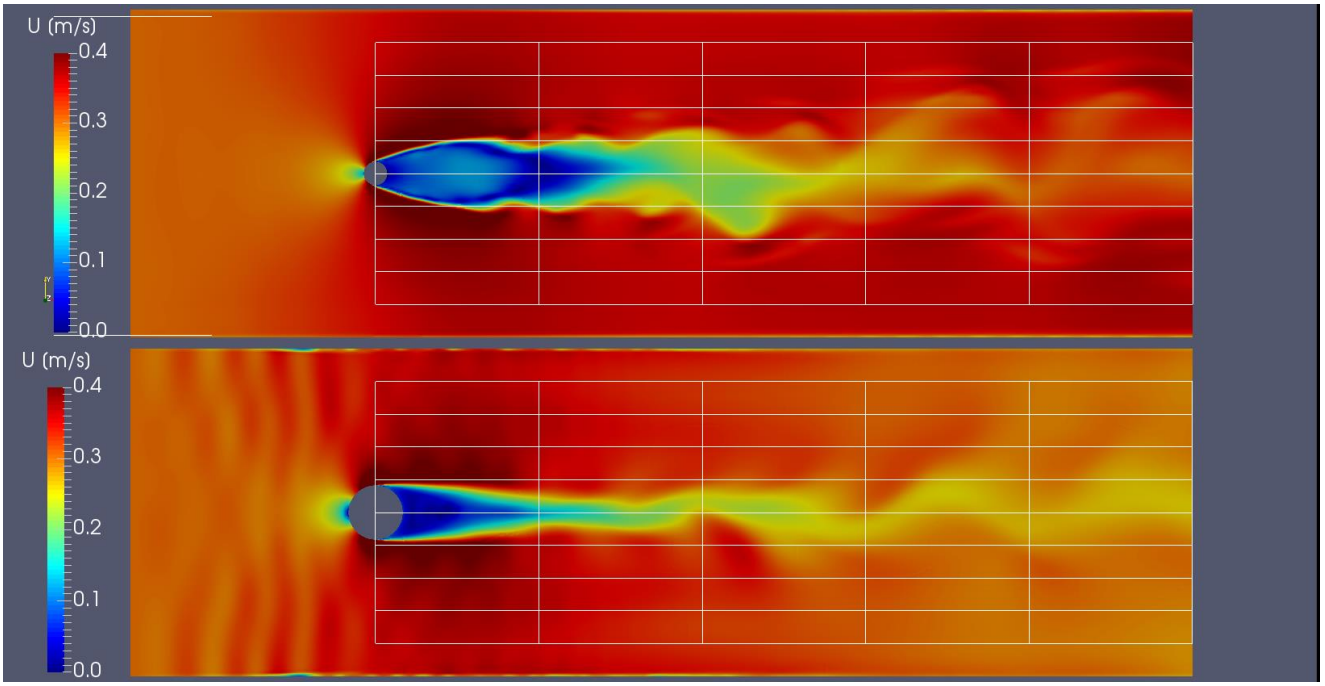

Figure 8.4: GBS, current speed at -5 and -25 m (top and bottom) after 4320 s. The grid is 400 m long and +/-80 m wide.

8.3 Influence area

The affected cross-section downstream the MP is approx. 50 m wide. Figure 8.4 shows the turbulence kinetic energy for cross-section at various distances perpendicular to the pile for the top 5 and the last one for the baseline. Immediately downstream the eddies generated a lot of turbulence and the energy is high over the whole water column to around 350 to 400 m downstream to a distance perpendicular to the flow direction of around 50 m.

It is also noted that the shear between the two layers generates turbulence kinetic energy in the same range as the downstream eddies. The main difference is the distribution. Where the turbulence between the layers is located in a band close to the stratification is the turbulence 50 m downstream the MP equally distributed over the depth for at 400 m to be even lower than the background.

Thus with a distance between the turbines between 1200 to 1600 m, the additional mixing will be 100/1400. The 100 m is the width of the area where the MP influence the mixing and the 1400 m is the estimated average distance between the MPs.

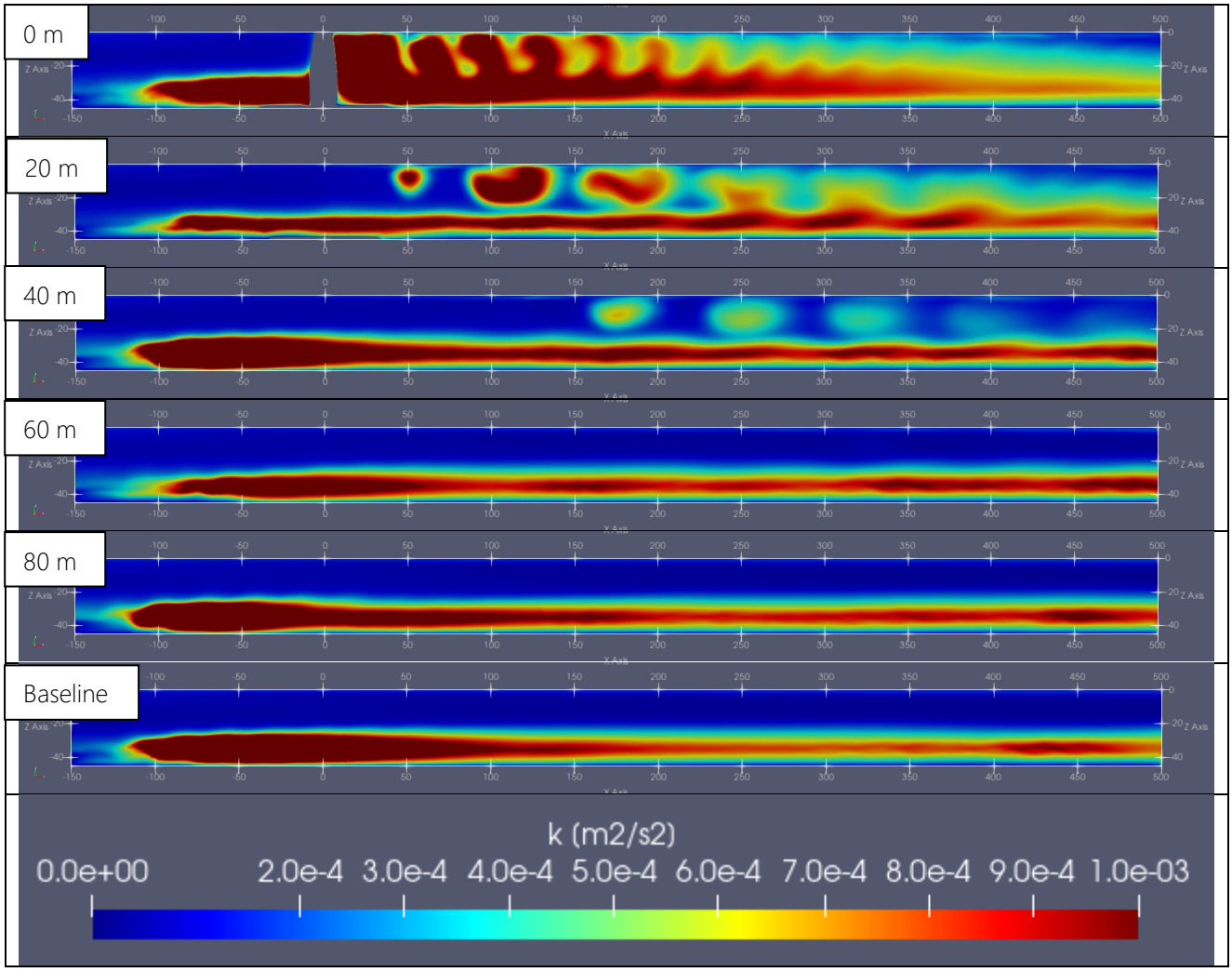

Figure 8.5: Event 1 after 5200 seconds, Turbulence kinetic energy, cross-section profiles parallel to the flow direction. From no. 1 to 5: 0, -20, -40, -60 and -80 m perpendicular to the location of the MP. No. 6 is the base case.

Similar to the above but for a cross-section 450 m downstream the monopile perpendicular to the flow direction Figure 8.5 shows also that the changes in the turbulence kinetic energy occur for around +/-50 m around the centre of the flume.

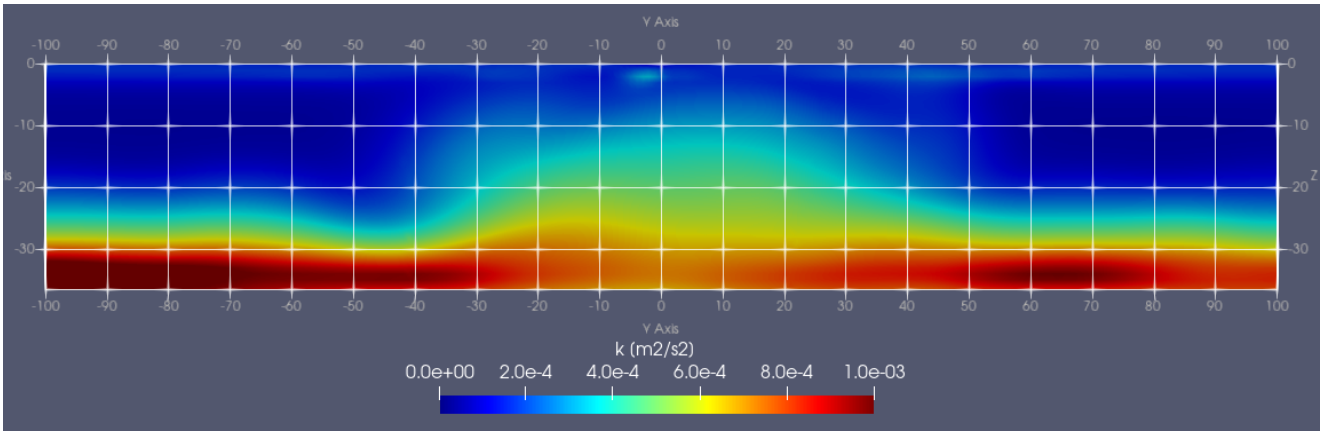

Figure 8.6: Event 1 after 5200 seconds Turbulence kinetic energy 450 m downstream the monopile.

8.4 Impact whole wind farm

The changes to the density compared to the situation without the presence of a structure are for a single monopile and a wind farm with 128 monopiles for the selected events estimated in Table 8.4. Moreover, as the events have various durations the impact has been scaled in time for an estimated of the average changes in the density.

The scaling from a single monopile is based on the assumption that the average distance between the foundations is 1400 m (chapter 4.2) and the affected distance is 100 m (chapter 8.3).

When scaled according to the duration of the individual events the average changes in the density downstream the wind farm is estimated to be 0.3 kg/m^3 corresponding to around 0.3 PSU in the temperature range from 5°C to 15°C. This 0.3 PSU is approximately in the same order as the daily variations in the salinity observed at the Arkona Buoy in the top layers and a factor 2 to 3 times less of the daily changes in the lower layers, Table 8.3.

Table 8.5: Changes to the vertical mixing after 5200 seconds 450 m downstream for a single monopile and 129 monopiles. For the single event and scaled according to duration.

Event	Duration, estimated	Changes in density			Single MP	All 129 MP	All 129 MP	
		Baseline	MP	MP vs. Baseline	Change in density	Change in density	Change in density, scaled to duration	
	[%]	[%]	[%]	[%]	[m^3/kg]	[m^3/kg]	[%]	[m^3/kg]
1	35.1%	6.3%	6.6%	0.3%	1005.03	1005.24	8.3%	0.02
2	32.2%	3.3%	4.0%	0.8%	1005.03	1005.28	8.9%	0.02
3	8.4%	0.3%	1.4%	1.1%	1005.08	1005.71	5.9%	0.04
4	2.9%	7.1%	10.9%	3.8%	1005.26	1007.43	7.1%	0.17
5	21.4%	0.0%	0.0%	0.0%	1005.00	1005.00	0.0%	0.00

The situation with the largest mixing is when the current speed in the top and bottom layer is in opposite directions, Event 4. It is rare which is estimated to occur for 2.9% of the time but will for this period increase the salinity with 3.1 PSU from 7.7 PSU to 10.8 PSU downstream the wind farm.

Event 5 where the current at the bottom layer is higher than the top layer shows no increase in the density probably due to a minimum amount of turbulence.

9 References

Baltic Sea Hydrographic Commission. (2020, 02 11). *Data*. Retrieved from bshc.pro

BSH. (2021, 10 10). *O-1.3*. Retrieved from https://www.bsh.de/EN/TOPICS/Offshore/Offshore_site_investigations/Procedure/O-01-03/O-01-03_node.html

ECMWF, C. C. (2019, 03 01). *Climate Data Store*. (ECMWF) Retrieved from https://cds.climate.copernicus.eu/cdsapp#!/dataset/reanalysis-era5-single-levels?tab=form

EMODnet. (2020). *Bathymetry*. Retrieved from portal.emodnet-bathymetry.eu

Fei-dong Zheng and Jian-feng. (2017). Study on the Critical Shear Stress of Cohesive Sediments. *IOP Conference Series: Earth and Environmental Science*.

Jacobsen, N., Fuhrman, D., & Fredsøe, J. (2012). A Wave Generation Toolbox for the Open-Source CFD Library: OpenFoam. *Int. J. Numerl. Meth. Fluids, 70*, 1073-1088.

Matrikelstyrelsen, K. &. (2012). Sea charts.

Miljøministeriet. (n.d.). *AIS data*. (Miljøministeriet) Retrieved 03 01, 2018, from http://www.dmu.dk/1_Viden/2_Miljoe-tilstand/3_samfund/AIS/

NIRAS A/S. (2021). *Triton Sediment Dispersal*.

OpenFOAM. (n.d.). *OpenFOAM*. Retrieved from https://www.openfoam.com/: https://www.openfoam.com/

SMHI. (2019, 10). *Ladda ner oceanografiska observationer*. (SMHI) Retrieved from https://www.smhi.se/data/oceanografi/ladda-ner-oceanografiska-observationer/#param=seatemperature,stations=all

SMHI. (2019, 09 01). *vattenwebb*. (SMHI) Retrieved from https://vattenwebb.smhi.se/station/#

U.S. Department of the Interior & U.S. Geological Survey. (2013). *Scientific Investigations Report 2008–5093*. (USGS) Retrieved 02 202, from https://pubs.usgs.gov/sir/2008/5093/table7.html

Appendix 1: Current roses yearly variations 2008 to 2018

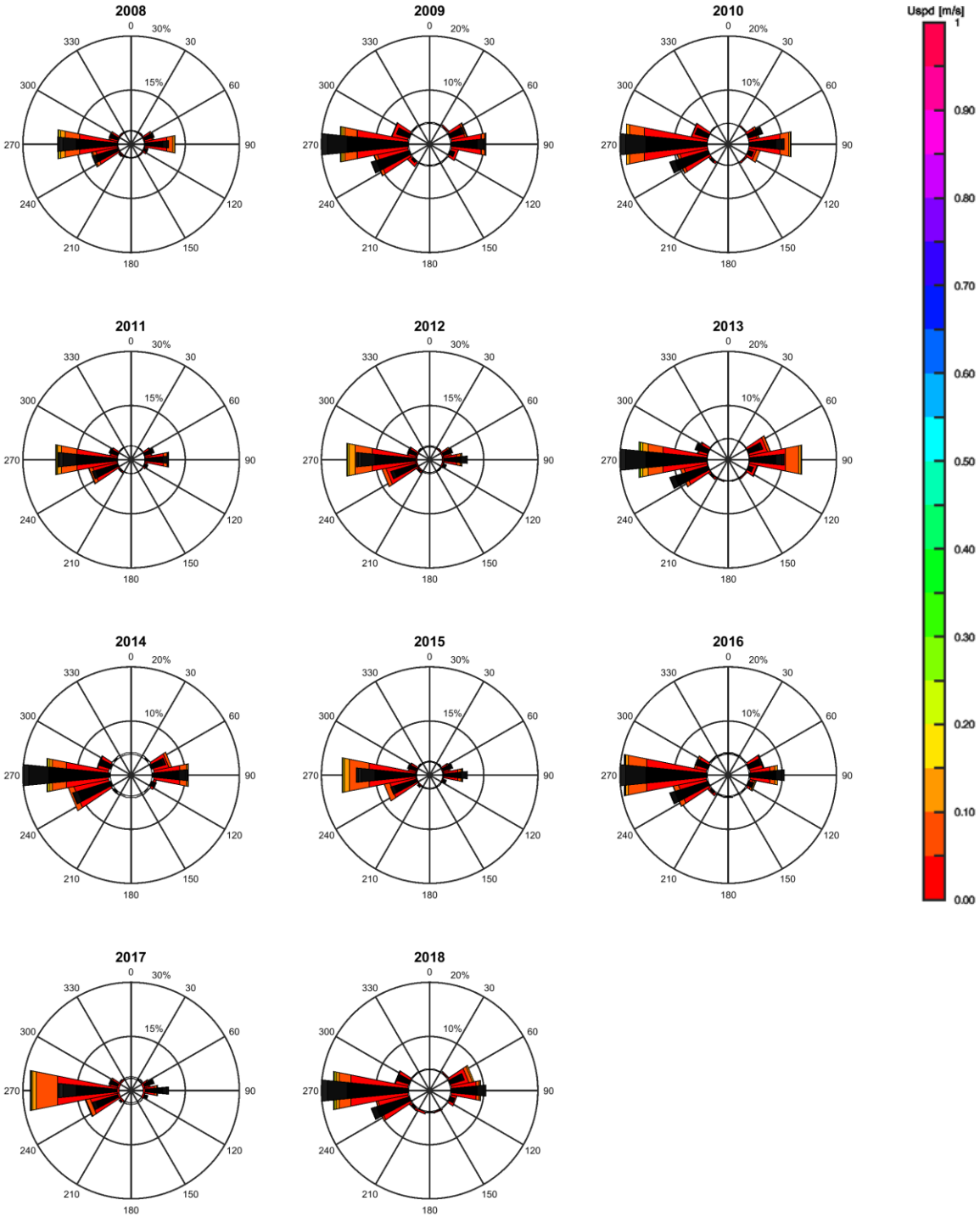

Appendix 2: Current roses monthly average year 2008 to 2018

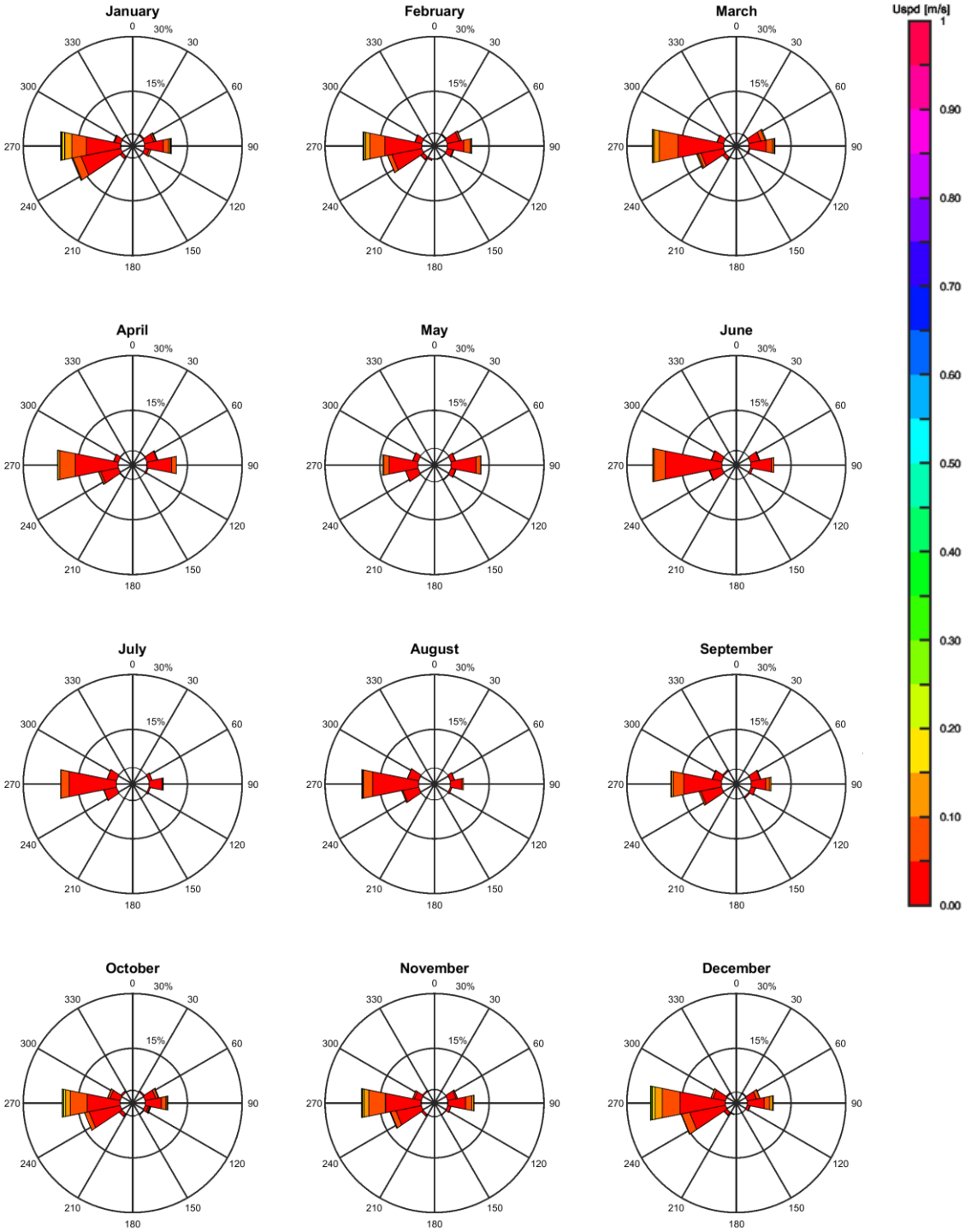

Appendix 3: Current roses April to December from 2008 to 2018

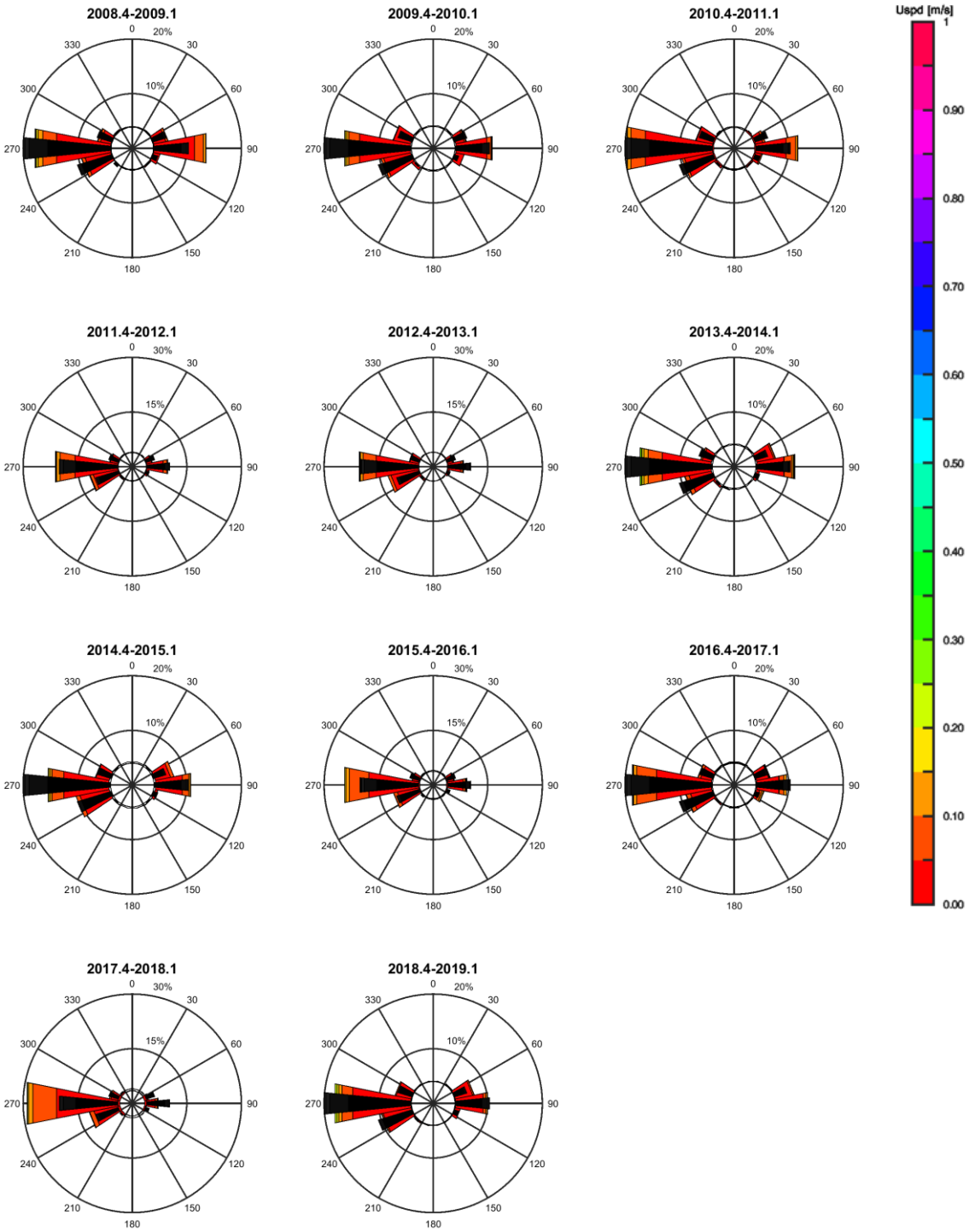

Appendix 4: Arkona, measured temperature 2014-2017

Black line = estimated location of the termocline (largest gradient)

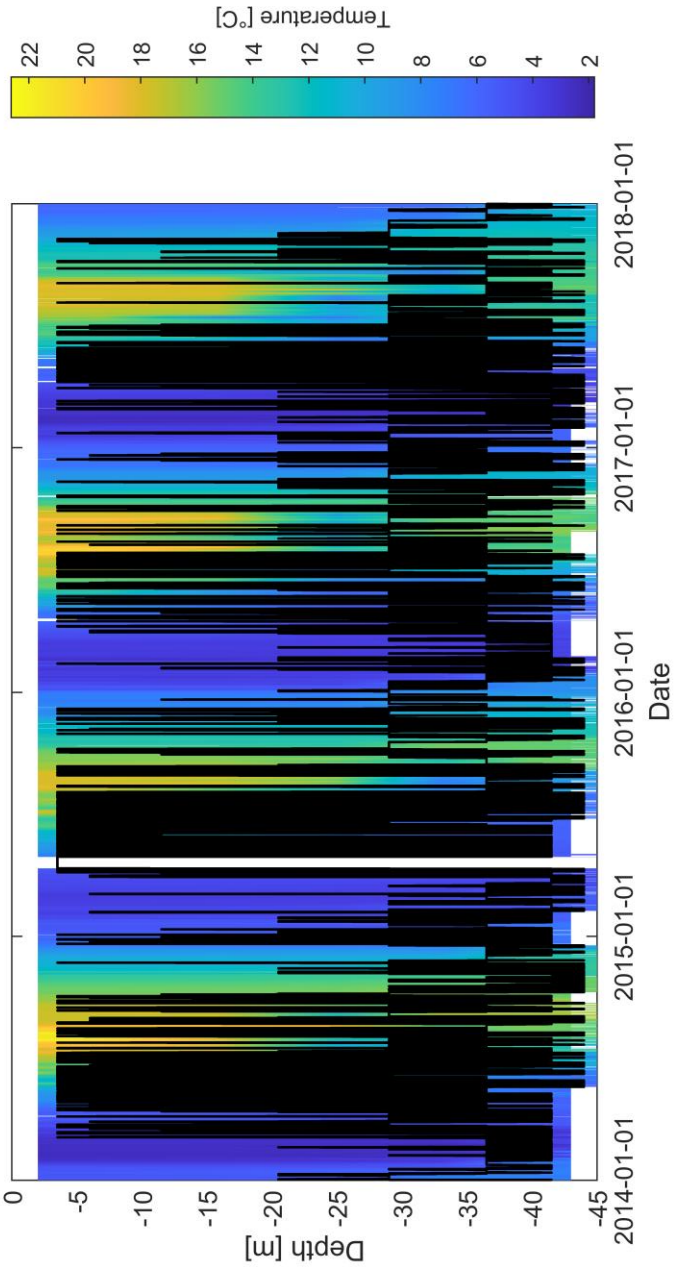

Appendix 5: Arkona, measured salinity 2014-2017

Black line = estimated location of the halocline (largest gradient)

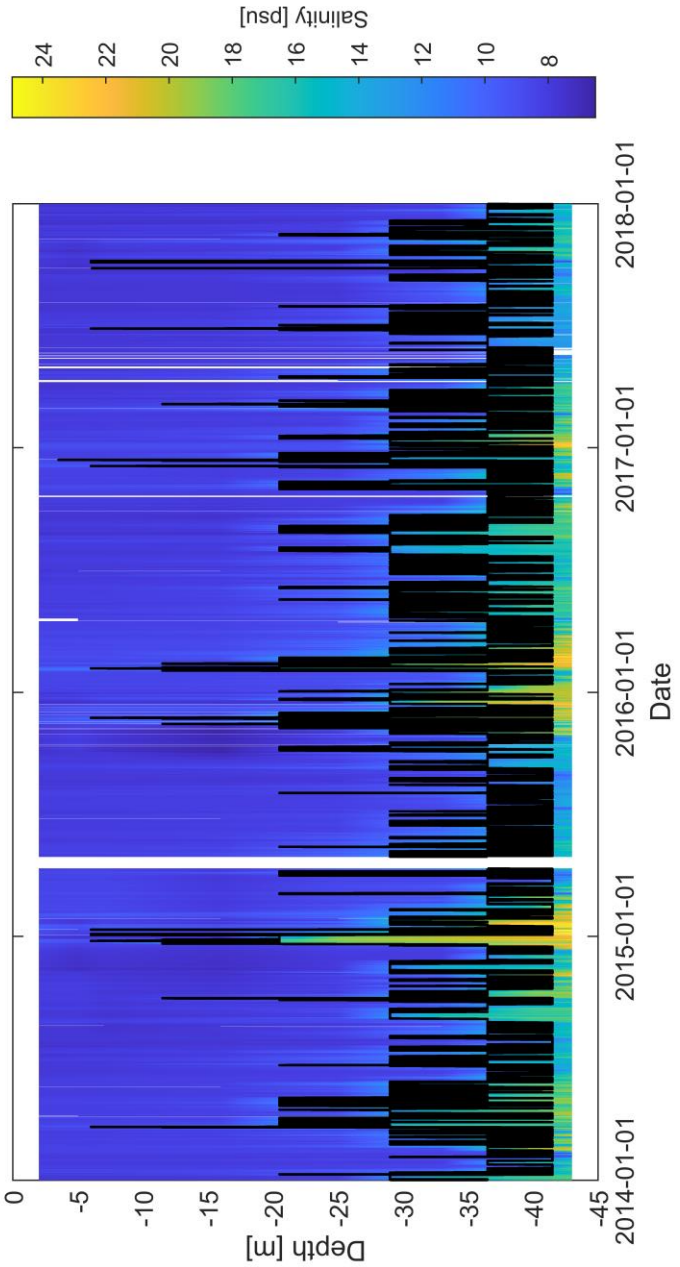

Appendix 6: Arkona, calculated density 2014-2017

Black line = estimated location of the pycnoocline (largest gradient)

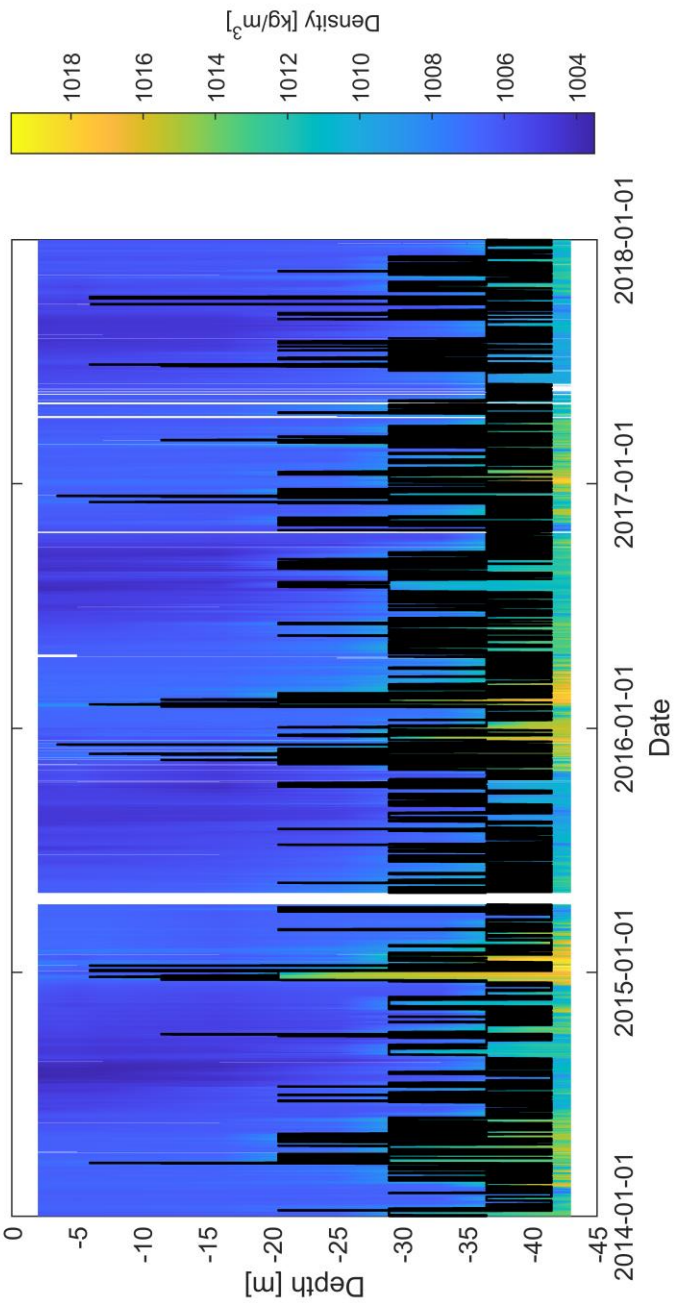

Appendix 7: Arkona, measured current speed 2014-2017

Black line = estimated location of the pycnocline (largest gradient)

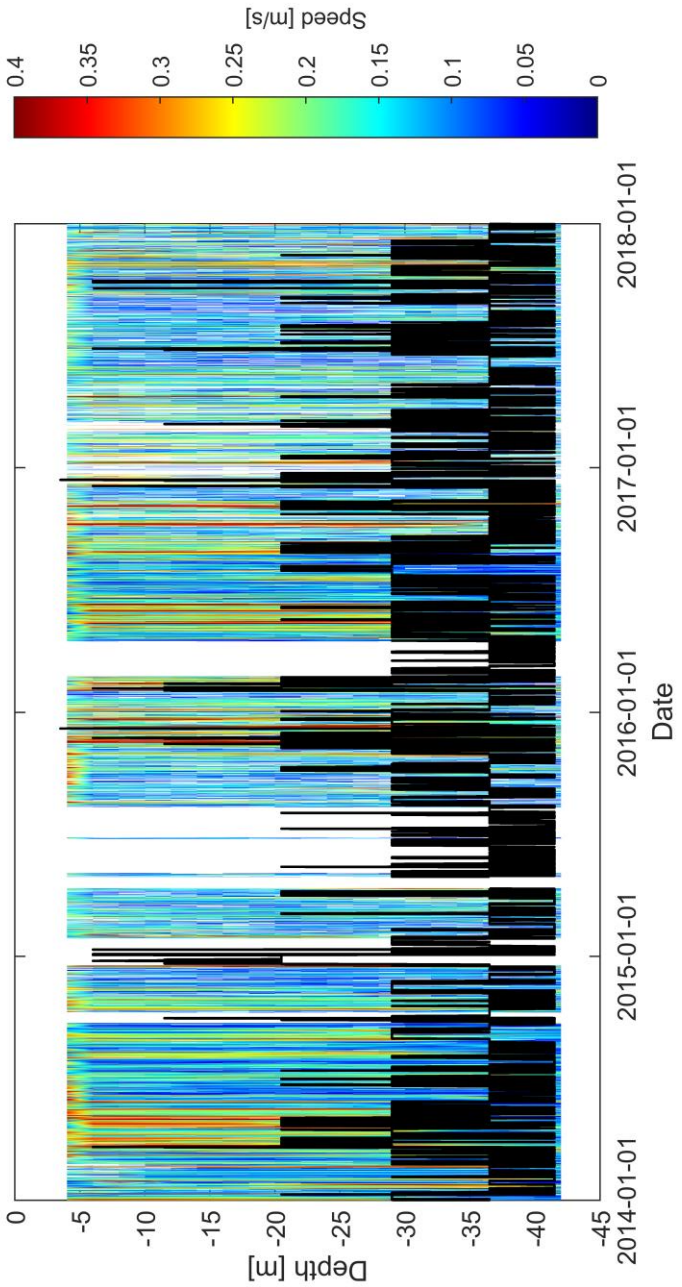

Appendix 8: Arkona, measured current direction 2014-2017

Black line = estimated location of the pycnocline (largest gradient)